Geochemistry, Geophysics, Geosystems®

AGU ADVANCING EARTH AND SPACE SCIENCES

RESEARCH ARTICLE
10.1029/2022GC010842

Multiscale Spatial Patterns in Giant Dike Swarms Identified Through Objective Feature Extraction

A. Kubo Hutchison[1], L. Karlstrom[1], and T. Mittal[2]

[1]Department of Earth Sciences, University of Oregon, Eugene, OR, USA, [2]Department of Geosciences, Pennsylvania State University, University Park, PA, USA

Key Points:

- Superimposed spatial patterns in dike swarms are revealed by the Hough Transform
- Deccan Traps and Columbia River Flood Basalts exhibit multiscale overlapping dike swarm structures
- Linear and radial mesoscale swarm structures are identifiable in Hough space

Supporting Information:

Supporting Information may be found in the online version of this article.

Correspondence to:

A. Kubo Hutchison,
akubo@uoregon.edu

Citation:

Kubo Hutchison, A., Karlstrom, L., & Mittal, T. (2023). Multiscale spatial patterns in giant dike swarms identified through objective feature extraction. *Geochemistry, Geophysics, Geosystems*, *24*, e2022GC010842. https://doi.org/10.1029/2022GC010842

Received 3 JAN 2023
Accepted 11 JUL 2023

Author Contributions:

Conceptualization: A. Kubo Hutchison, L. Karlstrom, T. Mittal
Data curation: T. Mittal
Methodology: A. Kubo Hutchison, L. Karlstrom
Software: A. Kubo Hutchison
Validation: A. Kubo Hutchison
Writing – original draft: A. Kubo Hutchison, L. Karlstrom, T. Mittal

Abstract Dike swarms are ubiquitous on terrestrial planets and represent the frozen remnants of magma transport networks. However, spatial complexity, protracted emplacement history, and uneven surface exposure typically make it difficult to quantify patterns in dike swarms on different scales. In this study, we address this challenge using the Hough transform (HT) to objectively link dissected dike segments and analyze multiscale spatial structure in dike swarms. We apply this method to swarms of three scales: the Spanish Peaks, USA; the Columbia River Flood Basalt Group (CRBG), USA; the Deccan Traps Flood Basalts, India. First, we cluster dike segments in HT space, recognizing prevalent linearly aligned structures that represent single dikes or dike packets, with lengths up to $10 - 30x$ the mapped mean segment length. Second, we identify colinear and radial dike segment mesoscale structures within each data set, using the HT to segment swarms into constituent spatial patterns. We show that for both the CRBG and Deccan Traps, a single radial or circumferential swarm does not well characterize the data. Instead, multiple and sometimes overlapping mesoscale linear and radial features are prevalent suggesting a complex history of crustal stresses. The HT can provide useful insights in a variety of geologic settings where many quasi-linear features, at any scale, are superimposed spatially.

Plain Language Summary Dikes act as pipelines to transport magma from the deep Earth to the surface where it can erupt. Some of the largest concentrations of dikes on Earth occur in ancient continental flood basalts (CFBs), areas of massive volcanic output, but the spatial complexity and scale of these dike swarms has been a barrier to understanding the patterns within. We develop a new method to characterize distributions of linear features, such as dike swarms, inspired by tools and algorithms from image processing. We apply this tool to two CFBs, the Columbia River Flood Basalt Group, USA, and the Deccan Traps, India, as well as a smaller swarm in the Spanish Peaks, USA. We find numerous small packets of aligned segments and larger, radial, and linear patterns of dikes.

1. Introduction

Dikes are a primary mode of magma transport in the crust, connecting deep mantle melting with crustal magma storage zones and sometimes surface eruptions (Gonnermann & Taisne, 2015; Rivalta et al., 2015). Dikes are sometimes known to spatially focus, across a variety of scales, into areas of high concentration known as dike swarms. These dike swarms may be associated with a single magmatic center such as the Spanish Peaks (kilometer scale) (Muller & Pollard, 1977; Odé, 1957) or extend to continental scale such as the Mackenzie Swarm (>1,000 km) (Baragar et al., 1996; Ernst & Buchan, 1997; Fahrig & Jones, 1969). On Earth, the largest dike swarms are usually associated with anomalous mantle melting events that result in Large Igneous Provinces (LIPs) or tectonic breakups, and thus record significant magmatic-tectonic events in Earth's history (Bond & Wignall, 2014; Ernst et al., 2021; Yale & Carpenter, 1998). Although we have observed a few instances of dike swarm emplacement in recent times (Ayele et al., 2007), we lack observations of active dike swarm of the scale that is often seen in the rock record, especially in the case of continental flood basalts (CFBs) (Bunger et al., 2012, 2013). Dike swarms have also been observed or inferred on other planets such as Mars, Venus and Mercury, indicating that these features are essential to the movement of magma in a terrestrial planetary body (Crane & Bohanon, 2021; Ernst et al., 2001; Grosfils & Head, 1994; Rivas-Dorado et al., 2022). Dike swarms also represent one of the most visually striking illustration of long-distance (10–1,000s of km scale) vertical and lateral magma transport from crustal magma reservoirs.

Field studies of exhumed dikes swarms have provided insight into the dynamics and complexities of dike swarms at a range of scales (Jolly & Sanderson, 1995; Morriss et al., 2020; Paquet et al., 2007; Ray et al., 2007). Dike

segment thickness varies from centimeter scale to 100s of meters while lengths vary from meters to 100s of kilometers or in cases such as the Mackenzie Swarms 1,000s of kilometers (Baragar et al., 1996). At the largest end of the spectrum, CFB dikes have been observed to be over 100 m wide and kilometers to 100s of kilometers long, considerably larger than dikes associated with Ocean Islands or arc settings (Karlstrom et al., 2017; Mittal et al., 2021; Morriss et al., 2020; Thiele et al., 2020). Dike widths have been proposed to follow power-law distributions (Gudmundsson, 1995) although their is continued debate over whether log-normal or Weibull distributions may provide better fits considering issues with sampling the smallest scale of igneous dikes (Glazner & Mills, 2012; Jolly & Sanderson, 1995; Krumbholz et al., 2014).

Dike width distributions have been proposed to be controlled by magmatic overpressure (Babiker & Gudmundsson, 2004; Gudmundsson, 2002), host rock rheology (Karlstrom et al., 2017; Krumbholz et al., 2014), depth of emplacement (Delaney et al., 1986), and the frequency of multiple injections within a single dike (Nicolas et al., 2008; Sheth & Cañón-Tapia, 2015). Some of these theoretical and field-based inferences have been tested by laboratory analog studies (Kavanagh et al., 2006, 2018). These studies have highlighted the critical role of crustal layering (both rigidity and density layering), topographic stresses, magma buoyancy, and magma inflow rate in controlling the spatial pattern of dike propagation (e.g., vertical vs. lateral propagation) (Kavanagh et al., 2015; Urbani et al., 2018). Despite uncertainties about how well single dike models extrapolate to large dike swarms with complex inter-dike interaction (Gunaydin et al., 2021), dike swarms have been widely interpreted in terms of paleostresses and as direct evidence of a transcrustal magma plumbing system (Mittal et al., 2021; Rivalta et al., 2015).

Remote sensing studies and field mapping have led to structural classifications of the largest scale structure of dike swarms (Ernst et al., 2001). Some dike swarms form radial or circumferential structures both focused on a localized center potentially associated with a magma reservoir or plume structure, while others are primarily linear bundles of subparallel segments. These two end members, which we will also focus on in this work, have largely been interpreted as representing two magmatic "states": (a) the stresses are primarily endogenous to the magmatic system (e.g., a plume head (Baragar et al., 1996; Ernst et al., 1995; Mège & Korme, 2004), magma chamber (Callot et al., 2001), or volcanic edifice (Acocella & Neri, 2009; Gudmundsson, 2006; Roman & Jaupart, 2014)) and (b) stresses are exogenous (e.g., tectonic stresses such as rifting (Buchan & Ernst, 2021; John et al., 2000)). Interpreted this way, the structure of dike swarms can illuminate the mechanism and driving forces of their emplacement (Mège & Korme, 2004), and provide a key tool for understanding the links between mantle melting, surface volcanism, tectonic rifting, and the LIP life cycle (Black et al., 2021).

Although it is clear that multiscale patterns exist in giant dike swarms, surface exposures of individual dikes are often dissected into individual segments due to erosion/exposure, topography, or limited physical access. This severely limits how we can directly infer the mesoscale (10–100 kms) and large scale structure (>100 kms) of dike swarms in a statistically robust manner from observations. For example, based on scaling analysis of Linear Elastic Fracture Mechanics (LEFM), dike segments in many databases are much shorter than predicted (Delaney et al., 1986; Morriss et al., 2020). At present, it is unclear if this mismatch is telling us something about the underlying magma transfer processes or is just a consequence of observational limitations. For dike segments data sets spread over large areas with many overlapping orientations, potentially spanning a long time, it is presently difficult to interpret the mesoscale structures in quantitative and statically rigorous manner. In this study, we address this challenge by developing a novel method to objectively link dissected segments and utilize tools from image processing to analyze mesoscale and large scale structure in dike swarms. Our work builds upon existing work analyzing dike swarm geometries in a number of terrestrial and planetary LIPs (Buchan & Ernst, 2021; Ernst et al., 1995, 2001, 2021).

To demonstrate the methods, we first study dikes of the Spanish Peaks region in Colorado, USA—an often cited example of small radial dike swarm—and then focus on the two large dike data sets: dikes of the Columbia River Flood Basalt Group (CRBG) and Deccan Traps Flood Basalts (DT). Given the large scale (100–1,000s of km), significant amount of overlapping dike orientations, and generally complex spatial patterns of dike segments, these two systems provide a useful test case to test and illustrate the utility of our analysis method. These two CFBs also represent some of the best studied Phanerozoic LIPs in the context of volcanic stratigraphy, geochronology, and magmatic processes (e.g., Camp et al., 2017; Mittal et al., 2021). We envisage that, if useful, our methods can be easily generalized to other dike swarm data sets on Earth (e.g., Mackenzie dike swarm) as well as Venus and Mars.

Our study specifically focuses on the following questions:

1. Do dike swarms mapped as distributions of many disconnected segments actually represent a smaller set of structurally continuous structures?
2. Are LIP dikes organized into coherent spatial patterns at a sub-swarm or swarm scale?
3. Do multiscale dike structures differ between the CRBG and Deccan Traps, and if so does this imply differences in emplacement mechanics?

To investigate these questions, we have developed a workflow for linking and clustering dike segments based on the Hough Transform (HT), an algorithm commonly used in image processing (Ballard, 1981; Duda & Hart, 1972; Hough, 1962). We then use Agglomerative Clustering to classify mesoscale groupings of dike segments in the Hough space (HS) (Everitt, 1980; Sneath, 1957). We show that this method increases the lengths of dike segments by up to 3 orders of magnitude and may better represent the true scale of dikes in geologic data.

2. Methods

2.1. Hough Transform

The HT is a feature extraction method extensively used in image analysis and computer vision (Duda & Hart, 1972; Hough, 1962). Originally designed to detect lines in images, the algorithm has been adapted to detect arbitrary shapes (Ballard, 1981). Although magmatic dikes are typically linear, they can curve as they propagate through different stress fields and thus depend on the length scale of the stress fields (Acocella & Neri, 2009; Davis et al., 2021). To illustrate the method, we will focus primarily on straight features in the present study and will not link dikes that curve along their length. Curving dike segments are removed in a preprocessing step before linking (due to the linearity filter). In practice, a majority of the LIP dikes are linear segments, and our choice does not strongly affect the overall results (Figure 2). A full extension to curved features is beyond the scope of the present study.

We use the HT to help accomplish two goals: first, to link short dike segments into longer dikes; and second to evaluate the mesoscale structure of the dike swarm. The HT is independent of Cartesian midpoint location allowing us to link dike segments together that are far away from each other. In the classic HT formulation, initially an edge detection method is applied to an image to find discontinuities that may constitute shapes or features (Ziou & Tabbone, 1998). Each edge point is then transformed according to the following equation (Duda & Hart, 1972):

$$\rho = x\cos\theta + y\sin\theta \tag{1}$$

where θ is angle from the x axis in counterclockwise direction, and ρ is the distance of a ray from the origin to the line defined by the point and θ. Lines in Cartesian space become points in HS; points in Cartesian space are curves in HS (Figure 1).

In the application here, we use dike segment maps derived from field mapping and remote sensing as data inputs. Each dike segment is pre-defined between two endpoints. We assume that dikes all represent straight lines (ignoring curving dike segments) and thus each dike segment is represented by a single point in the HS regardless of its length. For each dike segment in Cartesian space, we determine the angle (θ) using:

$$\theta = \tan^{-1}\left(\frac{x_2 - x_1}{y_1 - y_2}\right) = \tan^{-1}\left(-\frac{1}{m}\right) \tag{2}$$

where the dike segment is represented by its endpoints (x_i) and (y_i) $i = 1, 2$ and m is the slope of the line. Angle, measured in degrees, varies between −90° and 90°. The negative angles represent clockwise rotation from vertical (e.g., red line in Figure 1a) and the positive angles represent anticlockwise rotation (e.g., blue line in Figure 1a). An Hough angle of 0° represents a feature with North-South orientation or azimuthal bearing of 360°. Angles of −90° and 90° are equivalent representing a line of slope equal to zero or lineament oriented East-West. The perpendicular distance (ρ) is measured from a specified origin location and is calculated as

$$\rho = [(-m(x_1 - x_c) + y_1]\sin(\theta) = b\sin(\theta) \tag{3}$$

where b is the y-intercept of the line and either end point can be used to calculate ρ. The perpendicular distance ρ is measured in units of length and can be both positive and negative. Positive ρ indicates an intersection point to

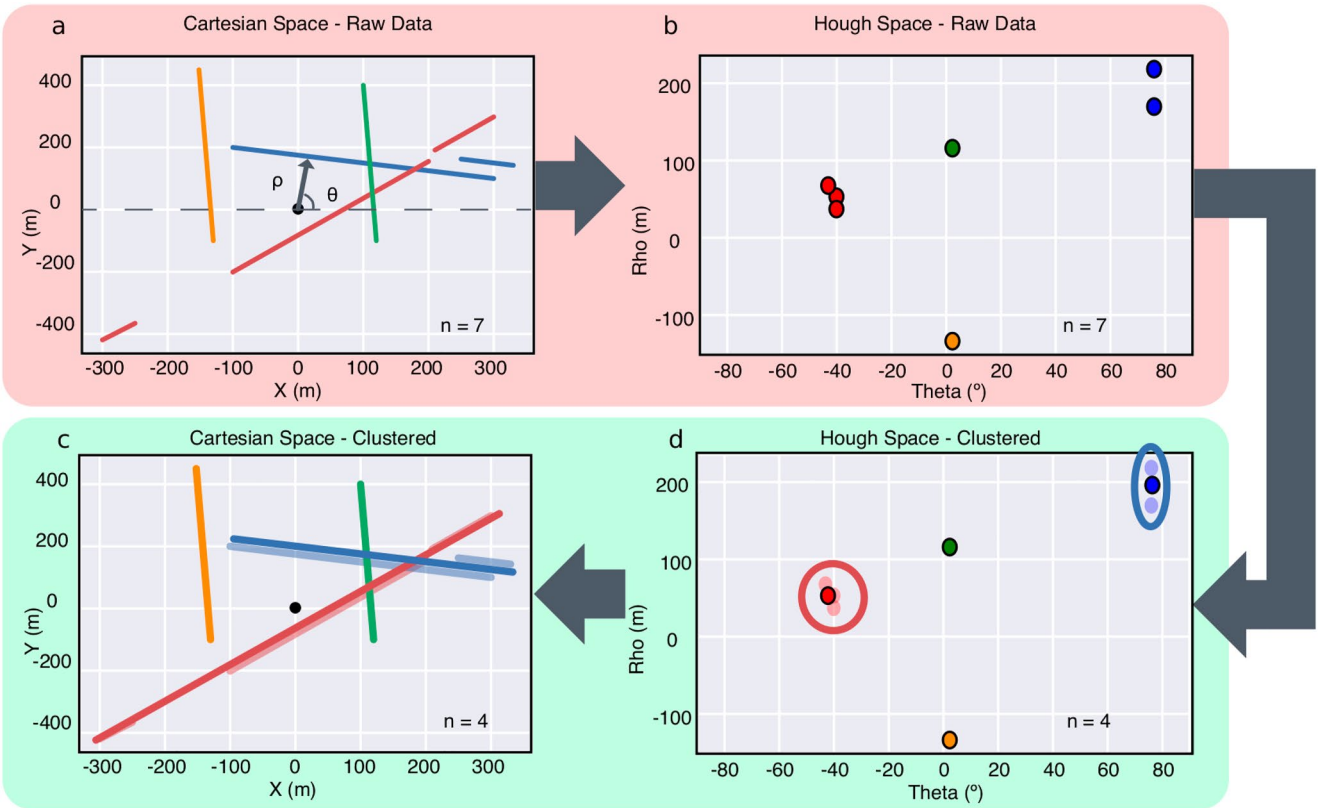

Figure 1. Dike linking algorithm using the Hough Transform. First, raw data in Cartesian space are converted into Hough space (a and b). Agglomerative clustering is then performed on the data in Hough coordinates (d), in this example there are four dikes total and two (red and blue) clusters. The clusters are redrawn by connecting the endpoints of the segments in the cluster (c).

the right of the chosen HT origin (e.g., red line in Figure 1a), while a negative distance indicates an intersection to the left of the origin (e.g., orange line in Figure 1a).

An important part of our method is to choose an appropriate origin for the HT, (x_c, y_c). The choice of origin modifies the resulting HS and the resulting clustering of line segments. By default we set the center of transform to be the average of the midpoints of the dike segments. While this choice is not unique, we have found that our default choice produces physically reasonable results.

2.2. Clustering Dike Segments

To link dike segments, we apply Agglomerative Clustering as implemented by the SciPy library on the Hough-transformed data sets (Müllner, 2011; Virtanen et al., 2020) (Figure 1c). Agglomerative clustering is a bottom-up hierarchical clustering method that recursively pairs samples together with the closest nearby cluster until a set distance threshold is reached, after which clusters will not be merged.

We chose Agglomerative Hierarchical Clustering (AHC) due to the multiscale structure of the dike swarms and the observational data set. On the dike scale level, field observations can include multiple segments of a dike structure oriented in the same direction. These segments have been unlinked due to exposure bias or small changes in surface expression such as en echelon segmentation. The dike scale is limited to the width of a "single dike packet" in the system. The other scale is the mesoscale structure of the dike swarm wherein the packets of dikes are aligned due to magmatic or tectonic stress. Analysis of the large scale dike swarm structure can provide information about these forces change laterally/temporally and thus the nature of the magmatic system. Given the hierarchical nature of clustering, the AHC algorithm allows data analysis on the two (or more) scales in a natural manner.

The AHC algorithm requires the choice of two parameters for unsupervised clustering. First, the linkage method which determines how the proximity between two objects in a cluster is calculated. We choose complete linkage

in which the proximity of two clusters is the distance between the two most distant objects (Sorenson, 1948) since we found that it consistently provides the accurate and noise-robust results for a range of synthetic dike data sets.

The second parameter is the distance over which the clusters will not be merged (d). We find that this is the most critical algorithmic parameter. The goal of our clustering analysis is to link segments that may be on the same line or along a narrow axis. Thus, we use a scaled Euclidean distance metric to determine the distance between data in the HS, scaling it by the angle cutoff ($\delta\theta$) and intercept cutoff ($\delta\rho$). For each data set, we choose strict angle cutoffs of 2° while setting the intercept cutoff to the mean length of the dike segments. We choose this limit because it is representative of the smaller segment-scale length in the databases. Our sensitivity analysis for the CJDS data set suggests that changing the ρ cut off has minor impact on the results (see Supporting Information S1 for full analysis). In contrast, changing the angle cutoffs can, unsurprisingly, affect the results significantly.

We set the distance cutoff (d) in the AHC algorithm to 1. This implies that if two points are exactly parallel ($\theta_1 = \theta_2$), their distances must be less than or equal to $\delta\rho$ from each other in order to cluster together. A schematic illustration of the AHC and dike linkage process is shown in Figure 1.

2.2.1. Robustness and Dike Characteristics

After linking is performed on the HS, we examine the clusters in both Hough and Cartesian coordinates for robustness. There are two ways in which transforming between HS and Cartesian space can introduce distortion. First, the difference between two values of the line ρ is approximately equal to the perpendicular distance between two parallel lines. However, there is distortion of this value in HS far from the Cartesian coordinate origin. In Supporting Information S1, we show that this occurs increasingly for large differences in angle but can be avoided by comparing only segments with similar θ. We combat this by choosing a coordinate origin which is the mean of segment midpoints and by breaking up the large data sets into regional subswarms. Second, in HS, lines with −90° and 90° have the same horizontal orientation (E-W from a map point of view). To solve this issue in HS clustering we simply rotate the data set so that the median angle is centered on 20°. This minimizes the number of clusters that cross −90° and 90° and 0° for the data sets of interest.

Finally, in the HS, lines are assumed to be infinite so the clustering does not account for where a segment falls on the line. We calculate a variety of metrics to give a sense of how the segments in a cluster are oriented to give a sense of structure. In Cartesian space, to find a new line segment to represent the cluster, we take the average orientation from all segments and extend the line so that it's tips represent the extremity of the individual segment endpoints.

We fit a rectangular box around the group of segments to find the dike segment "packet" length and the dike segment "packet" width, where the length is oriented along the packet orientation and the width is measured perpendicular to the length. *When referring to cluster length or width, we are referring to this measure and not individual segments*. As another measure of cluster distribution in Cartesian space, we calculate the maximum Euclidean nearest-neighbor distances between segment midpoints. This value is then normalized by the length of the cluster. For a cluster of only two segments, this number is always 1. For larger clusters, this number represents the distance between the two furthest segments. We assume that clusters where the two furthest segments are significantly far from each other, over half the length of the cluster, are less robust. *In subsequent analysis, we will refer to the subset of clusters filtered first by cluster size (>3 segments) and by the maximum nearest-neighbors distance* (<0.5) *as the "filtered" database*.

3. Data Sets

In this study, we have chosen three data sets to focus on and apply our methods. First, the Spanish Peaks which likely represents a volcanic edifice scale structure. Second, the Columbia River Basalt Group data set which includes four subswarms (Ice Harbor, Chief Joseph, Monument, and Steens) with the majority of our attention paid to the largest, the Chief Joseph Dike swarm (CJDS). Finally, we apply our method to the CFB province scale and examine the Deccan Traps data sets and the major subswarms (Central, Coastal, Narmada-Tapi, and Saurashtra) (GSI Bhukosh, 2020; GSI District Resource Map, 2001; Mittal et al., 2021 (accessed 1 December 2020)). The Spanish Peaks data set acts mainly as a test data set for our methods while we will compare the two CFB related swarms to investigate qualitatively the characteristics of CFB dikes. For each of the CFB data sets, the clustering is performed on the subswarm level to minimize HT distortion from the choice of an origin (refer to Table 1

Table 1
Hough Transform and Clustering Parameters for Each Data Set

Data set	Dike segments No.	Rho threshold (m)	HT center location (UTM)	Cluster No. (Total/Filtered)
Spanish Peaks	698	2,013	(−11684090, 4503618)	191/28
CRBG:CJDS	4064	433	(475083, 4976408)	1057/91
CRBG:Monument	103	1,201	(306813, 4943505)	20/1
CRBG:Ice Harbor	112	4,410	(369188, 5104698)	31/1
CRBG:Steens	61	408	(370992, 4721712)	10/1
Deccan:Central	5512	3,436	(8174542, 2237149)	1459/219
Deccan:Narmada-Tapi	11788	1,730	(8403558, 2495692)	2279/600
Deccan:Saurastra	8638	1,562	(7907507, 2440048)	2108/405

for specific clustering parameters). It is important to note that these data sets have been compiled from various sources (mentioned later). These include varying levels of ground truthing and information about dike thickness and ages. Thus, the presence and exact location of each dike segment in the database has not been verified in this study, but it is the best data currently publicly available. Certainly there are more unmapped dikes which have not been included and in some cases the mapping quality cannot be easily verified (Morriss et al., 2020). All the data sets and descriptions of the processing steps are available in Supporting Information S1.

3.1. The Spanish Peaks Dike Swarm

The Spanish Peaks area is located in southern Colorado in the Rio Grande Rift and is made up of two intrusive stocks and associated dikes in Tertiary sediments (Figures 2e and 2f). Spanish Peaks is one of the most commonly cited and studied radial dike swarm (Johnson, 1961; Odé, 1957). Spanish Peaks dikes exhibit three major components, first a radial structure centered on West Peak, a linear trend that strikes N. 60°E, and a secondary radial structure centered on Dike Mountain also known as Silver Mountain. Each intrusive body and the associated dikes represent distinct magmatic phases and compositions (Penn & Lindsey, 2009). The radial swarm of the Spanish Peaks is diffusely centered on West Peak although some dikes intercept outside the Peaks or in East Peak. West Peak is a quartz syenite dated to 24.6 ± 0.13 Ma while the East Peak is composed of granite and granodiorite porphyry dated to 23.9 ± 0.08 Ma (Penn & Lindsey, 2009). The dike compositions range from gabbro lamprophyre to granite porphyry (Johnson, 1961). The nearby Dike Mountain or Silver Mountain lies 50 km NW of the Spanish Peaks, and its associated dikes are syenodiorite (Johnson, 1961). Although the exact relationship between the two stocks and Dike Mountain is unclear, the Dike Mountain is dated as older than the Spanish Peaks intrusions (Penn & Lindsey, 2009). We chose to include these dikes in our database to demonstrate the algorithm's ability to differentiate between two closely oriented radial swarms. Using this full data set, we can also test our method's ability to devolve spatially overlapping radial and linear swarms. The dikes were digitized based on mapping in Johnson (1961) using QGIS software producing a shapefile of all dikes (linear and curving) which we have included in Supporting Information S1. These dike segments are then preprocessed using the steps described in Supporting Information S1. The final database used for clustering is available in Supporting Information S1 of this publication as a comma-seperated value file with well-known text (WKT) format for the dike locations.

3.2. Columbia River Basalt Group Data Set

From the CRBG, we investigate the Chief Joseph, Ice Harbor, Steens Mountain, and Monument dike swarms both individually and together as compiled in Morriss et al. (2020) (Figures 2a and 2b). The CRBG is the youngest flood basalt province on Earth and covers an area of approximately 210, 00 km^2 (Reidel, Camp, Tolan, Kauffman, & Garwood, 2013). Like other CFBs a majority of the CRBG was erupted in a short "main phase" pulse, 17.2–15.9 Ma with narrowing windows in progressive studies (Kasbohm & Schoene, 2018; Reidel, Camp, Tolan, Kauffman, & Garwood, 2013). Previously, dike swarms associated with CRBG have been linked together to form a radial dike swarm originating from an extensive centralized magma chamber in eastern Oregon (e.g., Camp & Ross, 2004; Glen & Ponce, 2002; Wolff et al., 2008).

The Ice Harbor subswarm is associated with post-main phase Saddle Mountain Ice Harbor flows dated ate 8.5 Ma (Reidel, Camp, Tolan, & Martin, 2013). The dike positions are inferred by high-resolution aeromagnetic survey

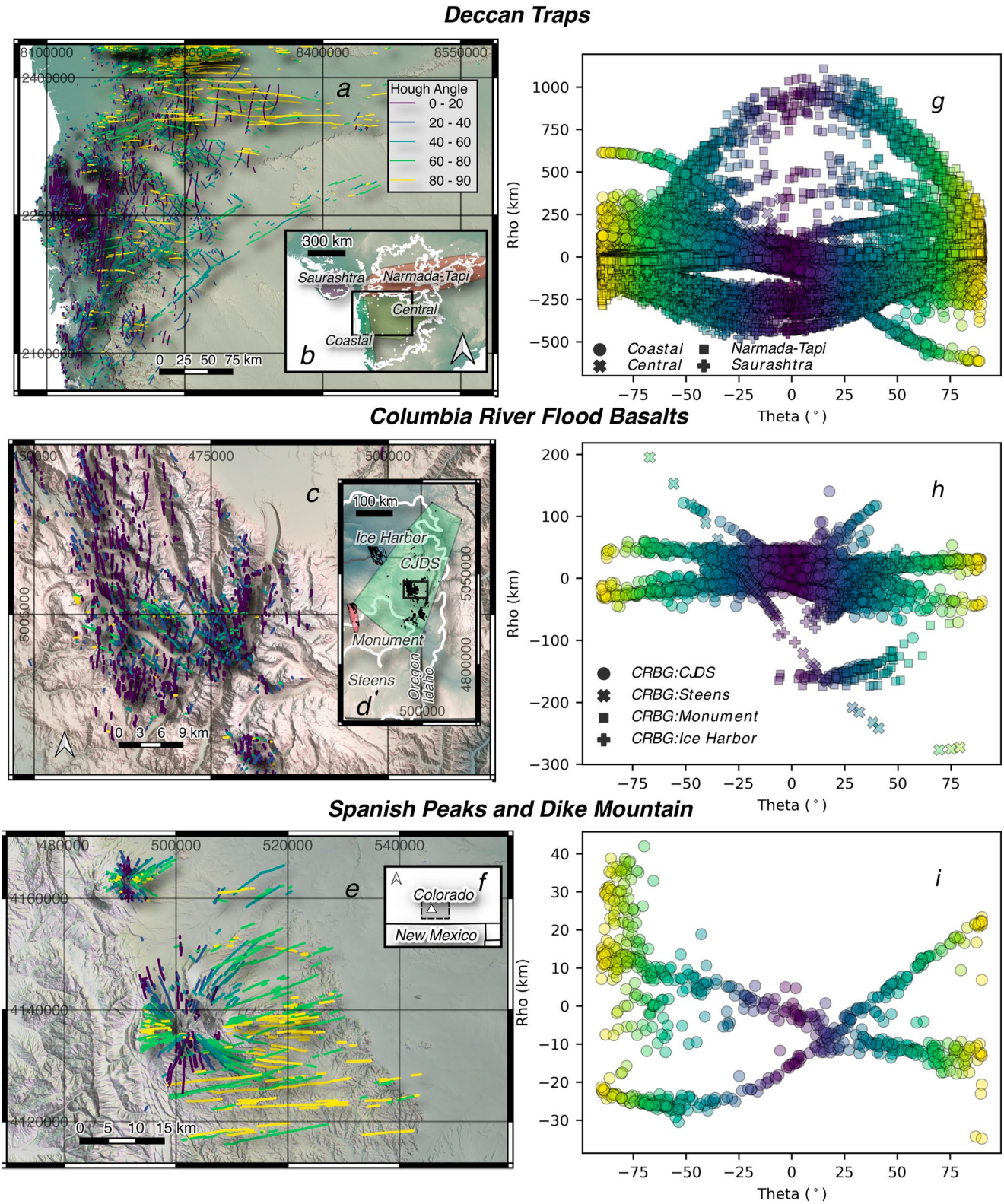

Figure 2. Map figures showing portions of the three data sets (a, c, e) with the large scale structure show in the insets (b, d, f) along with their respective structure in the Hough Transform space (g–i). All figures show the absolute value of the dike segment angle (θ) in degrees colored in terms of the colorbar in (a). White lines in the inset maps of (b and d) shows the extent of mapped lavas.

(Blakely et al., 2014; Morriss et al., 2020). The dikes appear mostly linear and strike N-NW at approximately 27 ± 11°. Monument dike swarm (Cahoon et al., 2020; Fruchter & Baldwin, 1975) located in central Oregon was mapped to have a similar orientation to the Ice Harbor swarm 30 ± 14°. Our Steens dike database consists of 69 basaltic dikes exposed on the flanks of Steens Mountain mapped by satellite imagery in Morriss et al. (2020). Steens dikes show a range of orientations and represent both the most southern exposures of dikes in the database. These dikes likely are linked to the CRBG's earliest eruption of the Steens Basalt (Kasbohm & Schoene, 2018; Morriss et al., 2020).

The largest of the CRBG associated databases, the Chief Joseph Dikes Swarm (CJDS) is mainly located in the Wallowa mountain regions of Eastern Oregon covering an area 100 km wide by 350 km long. The CJDS has been linked via geochemistry to the main phase formations of the CRBG: the Imnaha and Grande Ronde basalts. However, geochemistry has also revealed compositions spanning nearly the entire range of CRBG eruption members with the swarm (Morriss et al., 2020; Petcovic & Dufek, 2005). This suggests the area was a hub of overlapping intrusive activity for significant periods of time. This is also supported by the high segment density throughout the region of up to 5 segments/km^2. Overall, CJDS exhibits a linear orientation with strike NW at 6.0 ± 30°. However, significant secondary trends, offset in angle, are also present for the dike swarm which complicates the view of the swarm as singularly linear.

3.3. Deccan Traps Data Set

The Deccan Traps flood basalt consist of four main dike swarms the Saurashtra swarm, Narmada-Tapi, which extends from Saurashtra through the Mandla Lobe, the Coastal Western Ghats swarm, and east of that the Central Dike swarm or Nasik-Pune swarm (Mittal et al., 2021) (Figures 2c and 2d). The dike data set was compiled by Mittal et al. (2021) resulting in 29,000 dike segments based on a variety of sources including satellite imagery, district resource mapping, and digital elevation maps but the majority of segments are based from Geological Society of India field mapping (1:50k maps, (GSI Bhukosh, 2020; GSI District Resource Map, 2001 (accessed 1 December 2020))).

The western Narmada-Tapi region shows the highest density of dike segments and appears largely linear with ENE-WSW orientation along the rift-graben structure (Ray et al., 2007; Shukla et al., 2022). Dike segments decrease in frequency from west to east but are often clustered around rift-faults (Bhattacharji et al., 1996). The Saurashtra subswarm shares strong ENE-WSW orientation but also exhibits a range of angles. The Coastal Swarm, located along the Western Indian coast, shows a N-S orientation along the Western Ghats escarpment (Self et al., 2022a; Vanderkluysen et al., 2011). Finally, the Central or Nasik-Pune swarm shows little angle preference and has some of the longest individual segments lengths (up to 69 km, (Mittal et al., 2021)). In previous studies, the Central and Coastal swarms have been roughly separated by the Western Ghats escarpment. However, we choose to combine these two swarms due their large overlap in HT space and the presence of mapped dikes that cross this boundary (see Figures 2c and 2d). We will refer to it collectively as the "Deccan Central swarm" in the rest of the paper.

We anticipate that both the CFB data sets are likely incomplete due a combination of vegetation cover, lack of exposure, and the large areal extent. Thus, they are excellent candidates for our clustering algorithm to link individual dike segments. In both cases, the majority of outcrops occur at shallow paleodepths. The paleodepth of the CJDS is estimated to be ≈2 km (Morriss et al., 2020). The depth of original intrusions for Deccan is unknown but is also likely shallow (<4 km) since a large majority of the dikes are emplaced in either Deccan basalt or shallow basement (Ray et al., 2007; Sheth & Cañón-Tapia, 2015; Shukla et al., 2022). Many other giant dike swarms have also been shown to have relatively shallow to mid crustal depths of 6 − 15 km (Ernst et al., 1995). The limited vertical exposure limits the inferences about the deep crustal plumbing systems in CFBs. Nevertheless, the dike swarms are extremely important for understanding how magma is erupted from CFBs and thus what effects such voluminous eruptions would have on the atmosphere and biosphere.

4. Clustering Results

We applied the HT to dike segment databases from the Spanish Peaks, Deccan Traps, and CRBG then performed clustering in the HS to link clusters with similar orientations. In Figures 2g–2i, we show the corresponding data from the HT segment data for each of three data sets. As an example of what the algorithm does visually, we show

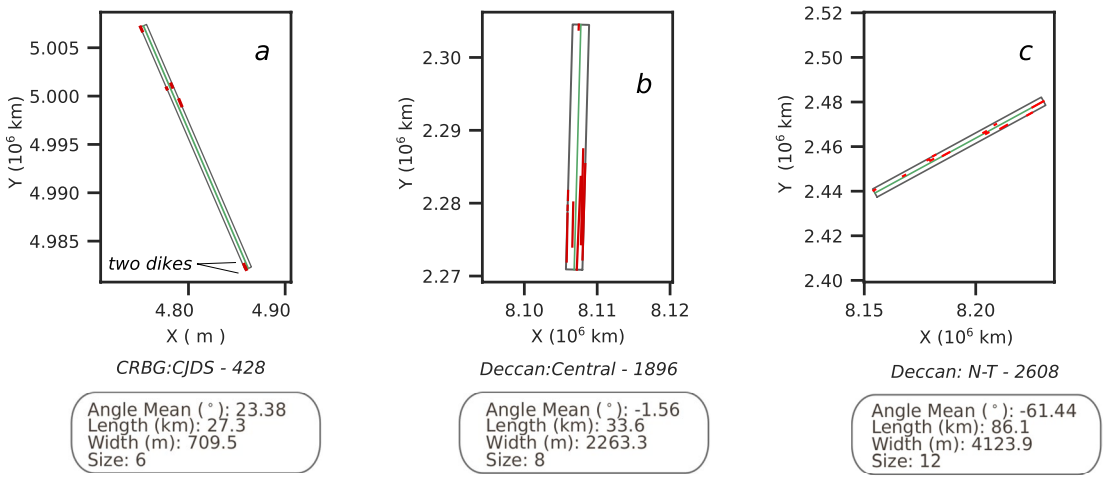

Figure 3. Example clusters from the Chief Joseph, Deccan Central, and Deccan Narmada-Tapi dike swarms (a–c respectively). The red lines show the mapped dike segments, the gray box shows a rectangle fitted around segments while the green line shows the average line of the cluster based on the Hough space orientation.

three representative examples of three clusters from the Chief Joseph, Deccan Central, and Deccan Narmada-Tapi dike swarms respectively (Figure 3).

For each data set, we see significant increases, by up to three orders of magnitude, in dike cluster length compared to the unclustered segment database (Figure 4). This is seen for all three full data sets and also at the subswarm scale. Furthermore, the filtered dike data set (clusters with size >3 and max nearest neighbors distance <0.5) are on average longer than the full clustered database. We do not account/incorporate clustered dike length in the filtering step and find that there is only a weak positive relationship of cluster size and cluster length (see Figure S3 in Supporting Information S1). We find that very long dike clusters (>200 km) have cluster sizes of 2–18 although clusters of over 5 are relatively rare (Figure S2 in Supporting Information S1). Overall, the results of our dike linkage analysis for the three data sets suggests that dike swarms mapped as distributions of many disconnected segments likely represent a smaller set of continuous structures.

The Deccan Traps dikes show the longest dike clusters with the extrema reaching over 1,000 km and a median length of 55 km (Figure 4). Although the individual segment lengths are roughly similar between the Saurashtra and Narmada-Tapi subswarms, the Narmada-Tapi swarm shows the longest linked dikes (1,100 km) of all subswarms, eclipsing even the longer segments of the Central swarm. The utility of our linkage algorithm is even more clearly exemplified for the CRBG data set. Before clustering, this data set had the short segments with an average length of only 400 m. However, after linking, the dike clusters have a median length of 10.6 km with some dikes reaching over 200 km (Figure 4). Within the CRBG data set, the Ice Harbor and CJDS show the longest lengths but we note that the Ice Harbor segments are inferred through aeromagnetic survey (Blakely et al., 2014) as opposed to field survey for CJDS data set.

The second scale over which we can evaluate diking activity is dike or cluster width. The median dike segment width observed in the CJDS data set is 8 m (Morriss et al., 2020). It is slightly higher for the Deccan dikes at 10 m, although the available segment width data on Deccan dikes is relatively sparse (Ray et al., 2007). After clustering, the Deccan shows higher dike packet widths (~2,300 m) than the CRBG (~700 m) or Spanish Peaks (~1,200 m). This is not surprising given the higher ρ clustering thresholds (see Section 2.2) for Deccan. Interestingly, the dike packet "width" is also the largest for the Narmada-Tapi swarm (~3 km) compared to ~2 km and ~1 km for the Central Deccan and the Saurashtra swarms respectively. This suggests that the longest Narmada-Tapi linked dikes are composed of a number of similarly oriented linear features.

5. What Do the Clusters Physically Represent?

Based on all our analysis above, we posit that the clusters found using our algorithm can present two possible interpretations: first, a cluster may represent a single fracture that is one continuous magma pathway including a set of en echelon fractures which have broken down due to rotations in the local stress field; second, it may

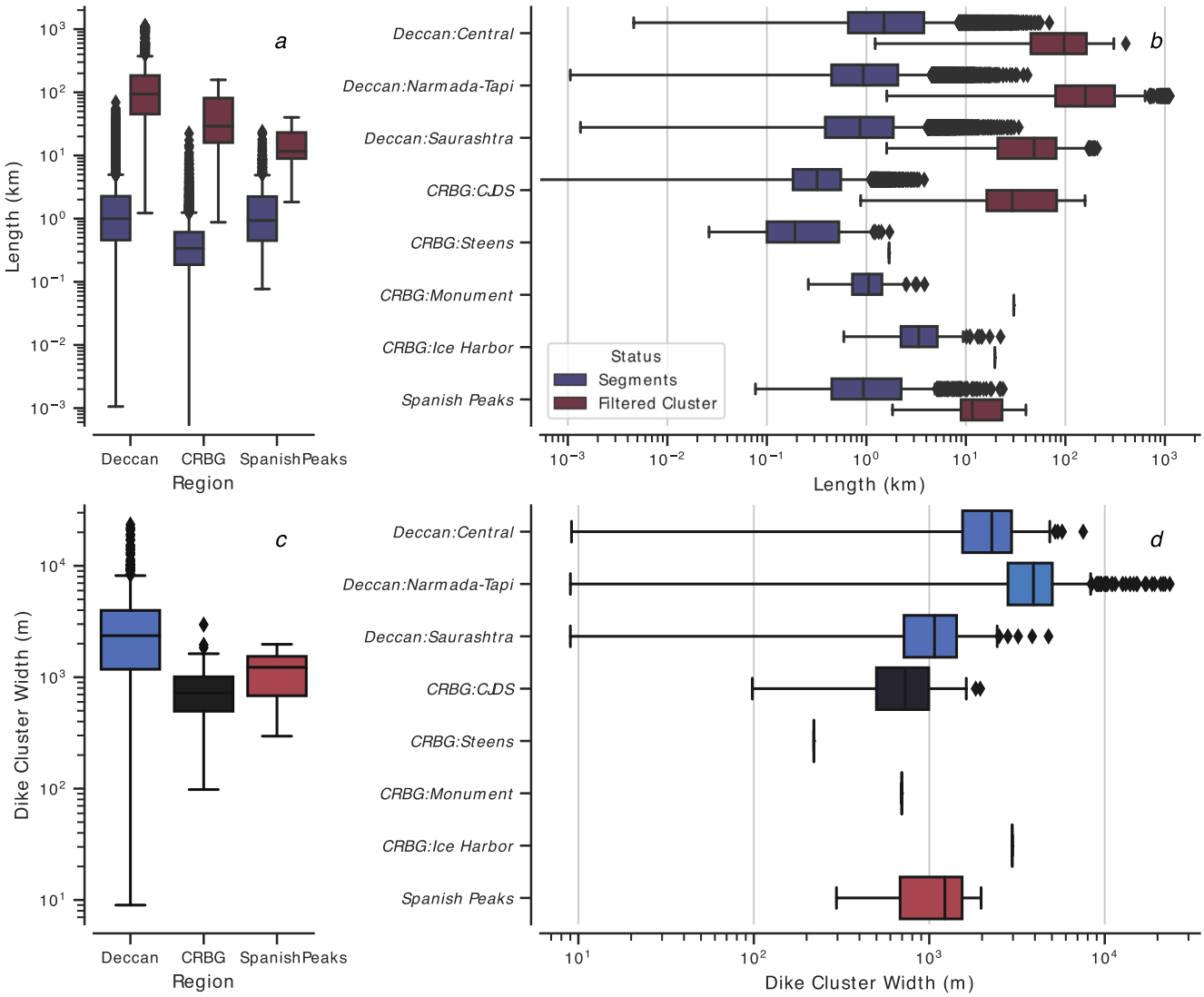

Figure 4. (a) Log-scale lengths of the segment database and filtered linked database in blue and red, respectively for the three regional databases. (b) Lengths broken down by subswarm for each region. (c) Log-scale widths of dike clusters found in the linked database, and filtered linked database in blue and red respectively for the three regional databases. (d) Dike cluster widths are shown broken down by subswarm for each region.

represent a family of fractures which may have been emplaced over long periods of time. Figure 3 shows examples of these different possible interpretations. Figure 3a shows short dike segments aligned on a narrow area with high aspect ratio. Figure 3b however shows many segments overlapping over a range of 2.2 km. Meanwhile, Figure 3c shows a long cluster (86 km) with many segments oriented evenly across it's length with some overlap. However, this still may not represent a single fracture but rather a series of related dikes emplaced over time, but being influenced by the same stress fields and re-using existing fracture pathways (from the previous dike). Whether the linked dike features represent lateral flow over 100 or 1,000s of kilometers in a single dike cannot be confirmed just with our linking method and requires further follow-up geochemistry and geochronology of the connected segments. However, our results clearly suggest that stresses are maintained over 1,000s of kilometers and for the duration of emplacement of the dikes.

5.1. Linear Elastic Mechanics Analysis

Dikes are classically modeled as isolated Mode I fractures (Rubin, 1995). Dike widths and lengths are related to each other based on the magma overpressure and host rock properties (Gudmundsson, 2002; Rubin, 1995). Using LEFM, the predicted scaling for the length to width ratio is

$$\frac{L}{W} = \frac{E}{2\Delta P(1-v^2)} \tag{4}$$

where L is the length, W is the width, E is the Young's Modulus, v is the host rock Poisson's ration, and $\Delta\Delta P$ is the magmatic overpressure. Using typical values, $E = 10 - 30$ GPa, $v = 0.25$, and $P = 1 - 10$ MPa), we expect this ratio to be $\sim 10^3 - 10^4$.

In Figure 5a we have plotted the dike cluster width and dike cluster length with three scaling ratio lines plotted over them (10^3, 10^1, 10^1) based on Equation 5. The CJDS data shows a bimodal distribution with one peak falling on the 10^2 line and the other falling between the 10^2 and 10^1 lines. The Deccan dikes are overall wider and longer than the CJDS dikes and fall mostly between the 10^2 and 10^1 lines but with a significant portion on or above the 10^2 ratio line. Breaking down the Deccan subswarms we find that Saurashtra subswarm shows overall shorter dike cluster lengths and widths more in line with the CJDS while the Deccan Central and Narmada-Tapi subswarms show significantly longer dikes. Overall, few clusters are close to the 10^3 ratio. Thus, we conclude that our dike clusters do not follow the expected LEFM predictions and are typically too wide. One potential explanation for the our results is that the effective crustal strength on large scales is weaker than the rock material properties due to presence of pre-existing fractures, thermal stresses from dike emplacement, and/or some viscoelastic stress relaxation (Eberhardt, 2012; Kavanagh & Pavier, 2014; Ma et al., 2020; Thiele et al., 2020).

To further evaluate intra-cluster distribution of segments, we examine predicted scaling for isolated dikes in a spatially variable (rotated) stress field, which often exhibit segmented or "en echelon" distribution (Pollard et al., 1982). To do this we look at the overlap between segments and the twist angle (Figure 5). Twist angle is calculated as the difference between the mean angle of the cluster and the line of best fit over the cluster midpoints. A twist angle of zero indicates the segments are aligned with the other segment endpoints. A higher twist angle indicates that the segments are offset from the line of their midpoints which could indicate en echelon type fracturing.

En echelon type fractures mix Mode I and Mode II type fractures associated with changes in the regional or local stress field due to material inhomogeneities (Pollard et al., 1982; Rubin, 1995). We calculate the total overlap across the cluster in meters then divide by the size of the cluster to find the average overlap per segment. Twist angle and overlap can be related together for en echelon type fractures using the following equation:

$$\mathcal{O} = l(1 - \cos(\omega)) \tag{5}$$

where $\mathcal{O}$ is the overlap per segment, l is the segment half length, and ω is the twist angle based on Equation 8b in Pollard et al. (1982) when the distance between segment midpoints is approximately equal to the segment half length. Due to the clustering parameters, the distance between two segments is necessarily less than the segment average length. On Figure 5d, we show this calculation for various segment half lengths which span the representative values for the different data sets ($b = 200$, 400, 1,000 m). Although some of the data is well represented by the lines, the majority of the data shows higher levels of overlap, or that the endpoints of dike segments within a packet are closer together. If the equation above holds true, this may suggest post-emplacement widening of the fractures by secondary processes as suggested in Pollard et al. (1982) or multiple generations of dikes being emplaced in the same areas.

The spacing between individual dike segments in a cluster (ρ) can also illuminate how the clusters were potentially formed. As a set of dikes fractures the host rock the energy necessary to maintain the growth of the dikes depends partially on how close they are together and how the strain of multiple dikes interact which is a topic of active research. Bunger et al. (2013) established a scaling analysis for the spacing of first generation fractures in a dike swarm and found it to be primarily dependent on dike height (H) since the further apart between fractures reduces the energy necessary to maintain the fracture. They found that for a dike with time variable magma supply, two potential scalings can arise: $\rho/H \sim 0.3$ or $\rho/H \sim 2.5$. Taking dike height to be approximately crustal thickness for LIP dikes ($H \sim 30$) and using the standard deviation of ρ in a cluster as the dike segment spacing, we find that our clusters do not follow the predicted ratio (~0.05, still less than predicted even for $H \sim 10$ km). This suggests that dike segments are closer together than theoretical models which may indicate that successive dike emplacement occurred between the first generation of dikes to maintain low interaction between newly forming fractures. Notably the cut off for clustering based on *deltaρ* is also significantly less than the (Bunger et al., 2013) scaling. Thus, our final conclusion isn't unexpected but it may support the idea that these clusters likely represent multiple generations of dike emplacement.

10.1029/2022GC010842

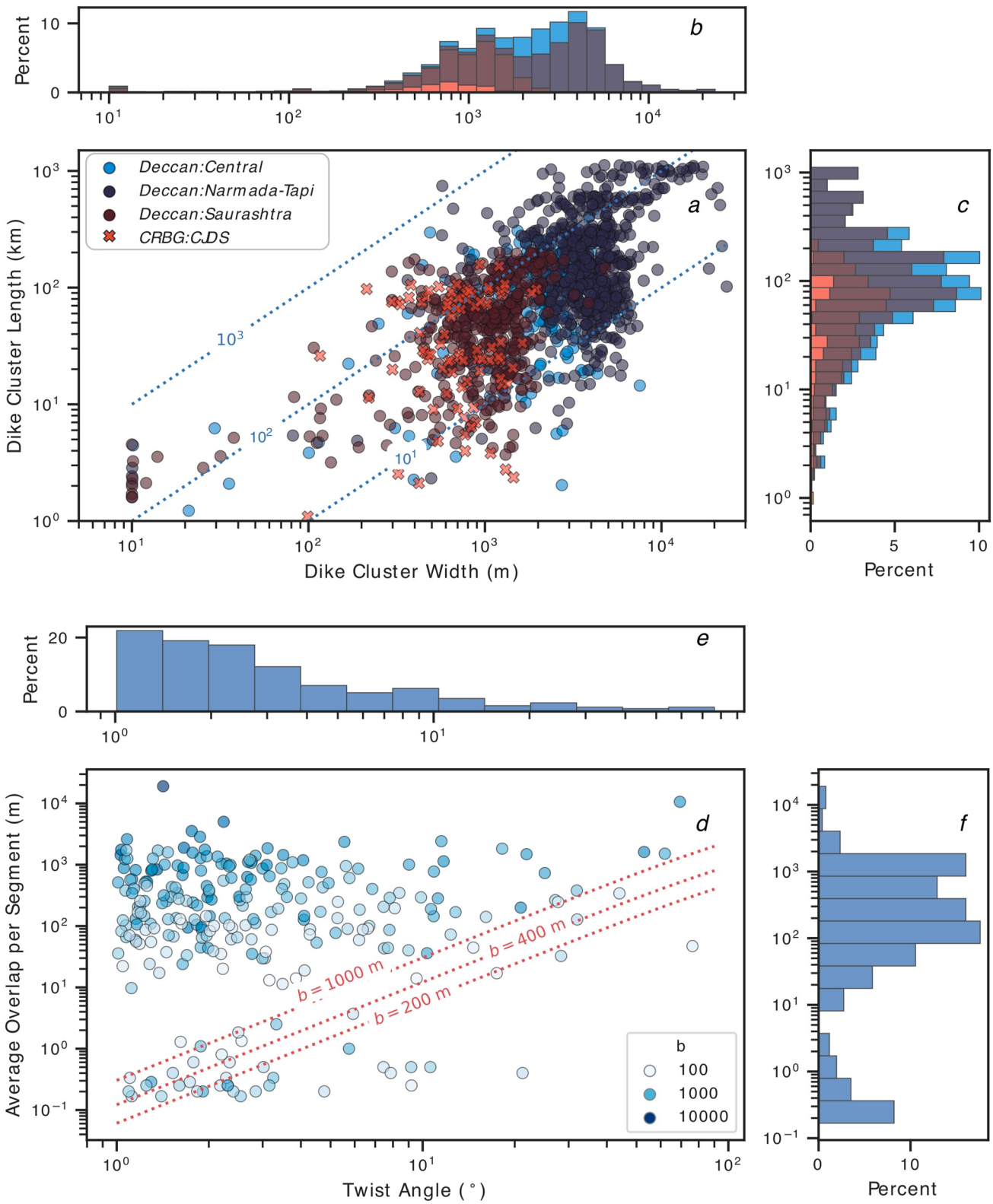

Figure 5.

5.2. Dike Swarm Associated Crustal Dilation

At a province scale, dilation due to diking can cause significant strain in the upper crust and has implications for the emplacement of the plumbing system and the crustal stress field (Thiele et al., 2020). Dilation is calculated as

$$D(x_i) = \sum_{n=1}^{N} \overline{w} \cos(\theta) \tag{6}$$

for the EW direction and

$$D(y_i) = \sum_{n=1}^{N} \overline{w} \sin(\theta) \tag{7}$$

for the NS direction where x_i and y_i are bins in the EW and NS directions, N is the number of dikes in each bin, $\overline{w}$ is the median width of the dike segment, and θ is the angle in HS. The average center of dilation is found by taking the weighted average of the bins using $D(x_i)$ and $D(y_i)$ as weights. These calculations can be performed for the segment or cluster database. The segment database provides a lower bound estimate of dilation while the linked clusters provide an upper bound, as long as our dike data set is reasonably complete. We used a typical segment width of 8 and 10 m for the CRBG and Deccan respectively (Morriss et al., 2020; Ray et al., 2007; Shukla et al., 2022).

The CRBG is dominated by EW dilation as is expected by the dominantly NS trending CJDS (Figure 6). The maximum dilation seen in the segment database (~1,300 m and ~1,000 m for the EW and NS dilation respectively) are similar in magnitude but on average EW dilation is higher. For the clustered data set however, maximum EW dilation significantly eclipses NS dilation (~3,100 m and ~700 m for the EW and NS dilation respectively). The Deccan data sets show dominant NS dilation with ~2, 800 m and ~10, 800 m for the segment and linked databases respectively (Figure 6). The EW direction showed lower amounts of dilation with ~2,500 m and ~4,600 m for the segment and linked databases respectively. This leads to a maximum strain of approximately 1% for both the Deccan and CRBG data sets in their maximum directions of dilation and 0.3% and 0.14% in the minimum direction of dilation respectively. Strain is calculated using the maximum dilation over the NS and EW ranges of each data set. Notably, in both LIP data sets, the area-weighted center of dilation implied by the clustered dike segments does not exactly align with dike outcrops (Figure 6 Dark blue dashed lines).

5.3. Summary Interpretation

In conclusion, dike cluster length does not necessarily represent one uninterrupted singular magma pathway or crack caused by fracturing (although in some clusters it may). Instead, dike packet width is likely the zone of influence that a dike may exert in the shallow crust. Dike clusters are indicative of sustained areas of diking activity from crustal magmatic system over a timescale when the regional stress field was relatively constant. Looking at the overlap within a cluster (Figure 5d), we see more overlaps than would occur in a simple en echelon fracture which may indicate that the observed overlaps are due to emplacement of multiple dikes in a zone of weakness over time by reactivation. Further, the continued magmatic emplacement in a localized region would reduce the crustal strength and introduce local stress heterogeneity that can further change the dike characteristics from the pure LEFM theoretical end-member. Notably, we are looking only at the end state of the magmatic plumbing system so the dike scale is integrated over the time of the activity.

Interpreting each cluster one-by-one is beyond the scope of this paper and would require other information about the dike segments such as geochemistry, paleomagnetic or radiometric dating, and more detailed field observations. Dating of the dike segments could establish whether the segments were formed in the same pulse of magma or if it was emplaced over long periods of time. Geochemistry can change along the length of the dikes Morriss

Figure 5. (a) Log-scale widths of dike clusters plotted against the log-scale dike cluster lengths. Three trend lines (blue dashed lines) are plotted over the data showing length to width ratios of 10^3, 10^2, 10^1 with the majority of the data plotting between the 10^3 and 10^2 trend lines. Despite these different values, the median aspect ratios are similar 53 versus 48 for the Deccan and Columbia River Flood Basalt Group, aspect ratio calculations are available in Data Sets S1–S4. (b and c) Shows the distribution of the dike cluster widths and lengths respectively. (d) Plots the twist angle in degrees versus the calculated average overlap per segment in meters (log-scale) only for a subset of the data ($n = 256$) which has twist angle of over 1° and overlap of over 0.1 m. The color of the dots indicates the half-segment length (b). In red dashed lines, three trend lines are plotted over the data indicating b values of 200, 400, 1,000 m, which are representative of average values seen in the different data sets. (e and f) Shows the distribution of twist angle and overlap respectively.

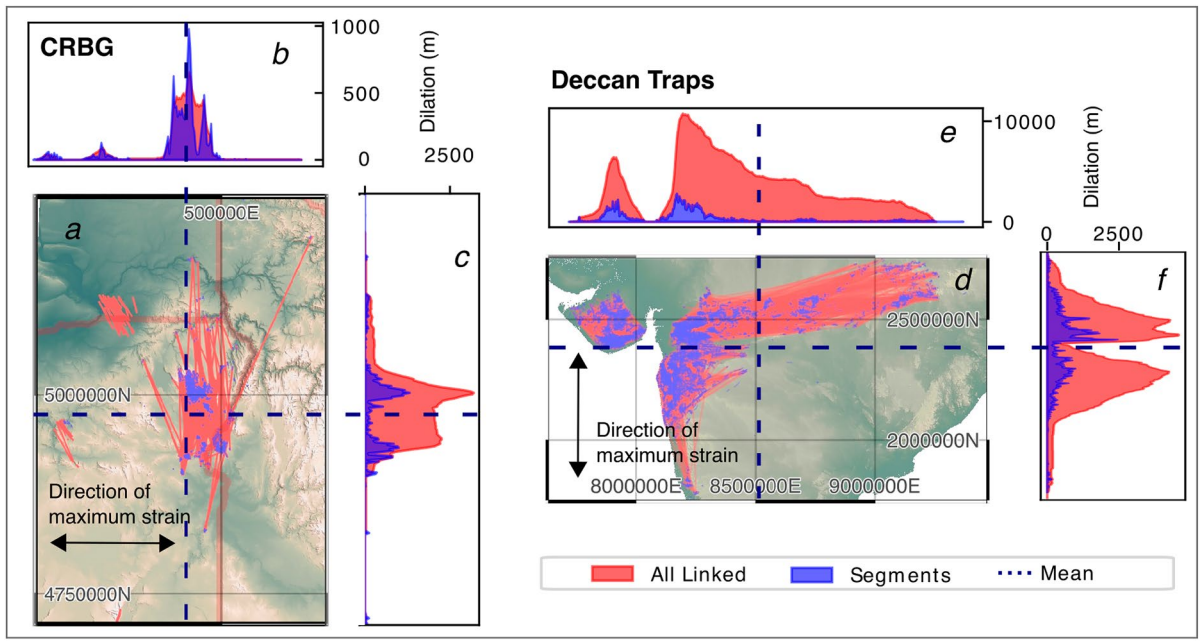

Figure 6. The left panel shows the CJDS while the right shows the Deccan dike swarms. (a and d) Shows the segment database (red) overlaid on the linked clusters (blue) while the two side panels (b and c). And (e and f) shows the dilation in the NS and EW directions for the segments and linked clusters of the Columbia River Flood Basalt Group and Deccan data sets respectively. The dark lue dashed line shows the segment density weighted center of dilation.

et al. (2020) but can be used to link dikes to crustal storage and transport. Any additional data could be added to the clustering algorithm for a higher dimension of clustering. However, our analysis suggests that clusters generally represent multiple generations of dikes aligned along narrow axes of activity. This interpretation of large CFB dike swarms provides supporting evidence for a trans-crustal, multi-magma reservoir magmatic architecture model for CFBs (Mittal & Richards, 2021). The spatio-temporal patterns in dike swarms may reflect an integrated lifecycle rather than a single time snapshot of the magmatic system (Black et al., 2021).

6. Structure of Dike Swarms in Hough Space

A key motivating question for our work is whether LIP dikes are organized into coherent spatial patterns at a sub-swarm or swarm scale. Spatial structure of dike swarms provides important constraints on dike-stress field interactions and external drivers of dike emplacement. Magma chambers (Gudmundsson, 2006; Karlstrom et al., 2009), regional tectonic stress (Wadge et al., 2016), and topography such as edifices (Roman & Jaupart, 2014) have been inferred based on mesoscale patterns in the dike swarms. We show that the HT can be a useful tool in evaluating a range of structures in both the segment and linked databases, providing a means to overcome often incomplete and discontinuous observations.

6.1. Synthetic Mesoscale Structures

We will first focus on two end members of mesoscale dike swarm structure: linear and centrally localized (Figures 7a and 7b respectively). Roughly these two regimes represent either a spatially consistent least principal stress axis, such as implied by tectonic extension (Wadge et al., 2016), or a radially symmetric stress field such as implied by a magma chamber, volcanic edifice, or mantle plume head (Ernst et al., 2001). Centrally localized swarms can include both radial and circumferential swarms. These two end members can coexist spatially if the stress field changes with time. Of the two, radial swarms are more challenging to robustly identify in Cartesian space because apparent radial structure can arise from multiple misaligned linear swarms (e.g., Figure 7b). These two end members are more easily identified in the HS where a linear swarm is represented by a vertical bar of points (Figure 7a) and a radial swarm can be seen as a sinusoidal curve spanning a sufficiently large range of angles. This is illustrated in Figures 7b and 7c, with synthetic line segment distributions. We also show some more complex swarm shapes and the associated difference in HT space shapes (Figures 7d–7f). The synthetics illustrate that HT space is very useful to distinguish amongst different kinds of dike mesoscale structure, although we focus only on end member patterns here.

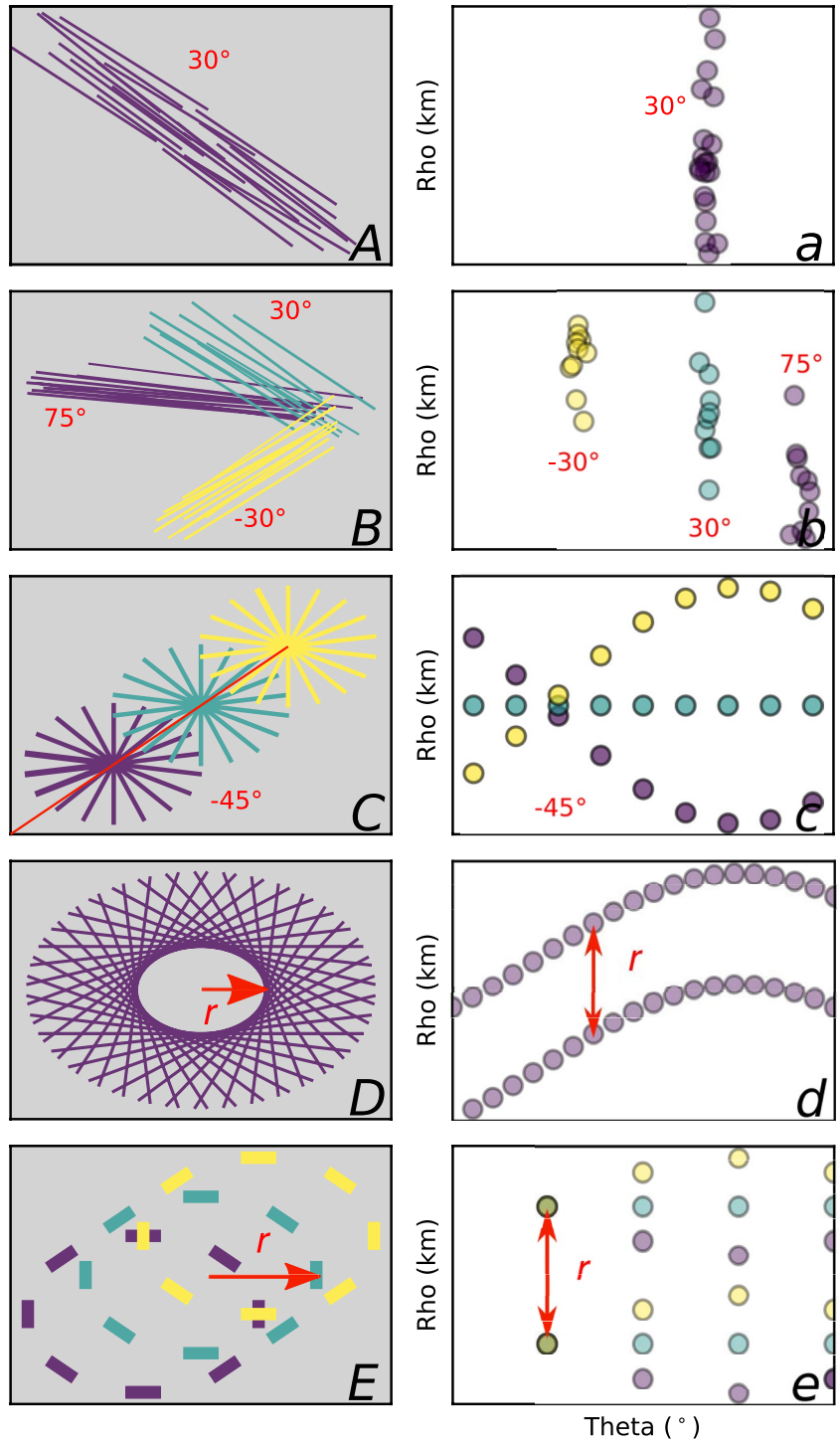

Figure 7. Synthetic dike swarms in a Cartesian space (gray background, uppercase label) and Hough Transform space (white background, lowercase label). (A) Shows as simple linear swarm oriented at 30°. (B) Shows three linear swarms at −30°, 30°, 75°. (C) Shows three radial swarms aligned at a −45° angle. The angle at which radial swarms intersect in the Hough space (HS) is the angle of their relative orientation in Cartesian space. (D) Shows a circumferential swarm with the lines extending to show how it converges to Equation 8. The radius of the circumferential swarm is equal to the spacing of the parallel two curves in HS. (E) Shows three circumferential swarms with the same radius aligned at −45° angle.

We use several criteria to distinguish ideal radial dike patterns from other structures. First, we require that a radial dike distribution has a range of constituent angles. Second, we assume that the structure has a small common area of dike intersection for interpreting this pattern as arising from a common magma source. To identify radial dikes, we return to the formulation of the HT in Equation 1 and find an equation for a perfectly intersecting radial distribution of segments

$$\rho_r(\theta) = (x_r - x_c)\cos(\theta) + (y_r - y_c)\sin(\theta). \quad (8)$$

where x_r and y_r are the Cartesian location of the radial center adjusted by the chosen origin of the HT. Using Equation 8 we can fit data in the HT space and find (x_r, y_r) a non-linear least squares to fit as implemented in Scipy Optimize library (Virtanen et al., 2020). We can then pick any line which falls within $\rho_r(\theta) - R_{\max} < \rho(\theta) < \rho_r(\theta) + R_{\max}$ which effectively draws a circle with radius $R_{\max}$ around the points (x_r, y_r) in Cartesian space and an envelope of half-width $R_{\max}$ around the line calculated in Equation 8.

Similar to ideal radial swarms, circumferential swarms form sinusoidal waves across HS with the center of the swarm described by Equation 8 (e.g., Figures 7d and 7e). However, in the case of a circumferential swarm there are two distinct and parallel sinusoidal waves at $\pm r$ where r is the radius of the circumferential swarm. To see why this is the case we show in Figure 7d that extending the lines of a circumferential swarm makes it appear similar to a radial swarm but without a point of intersection at the middle. Note again that the HT does not include information about where the segments falls on the infinite line which would differentiate the radial and circumferential swarms. The two trends seen in the circumferential case are separated by the radius of the swarm. Like the radial swarm, changing the center of the swarm changes the representation in HS as does changing the radius. For the circumferential swarm both the center and the radius has an effect on the HS representation whereas only the center effects a radial swarms representation (Figure 7e). For both types of centrally localized swarms the center can be found in the HS by fitting Equation 8 to the data. In the HS for a data set with limited or sparse segments, it may be difficult to distinguish radial from circumferential swarms. However once the sinusoid is identified and fitted it can be inspected in Cartesian coordinates to determine which end member is appropriate. An advantage of using the HS is that it allows the observer to isolate structures of certain orientations, and then inspect them for interpretation in Cartesian coordinates. By combining both parameter spaces, we can better understand complex overlapping patterns in the dike swarm and quantify the meso-scale structure.

Limitations of this method arise when the space over which line segments are spread is very great. Analysis of synthetic tests of radial swarms indicates that it is difficult to distinguish radial structures with centers whose distance in Cartesian coordinates is more than 2X the standard deviation of ρ from the HT origin (see Text S3 in Supporting Information S1). To account for this after fitting a radial swarm to the data one must both inspect it in Cartesian space and then recenter the HT on the radial center and run the fit again or cut the data into smaller sections to account for distortion.

6.2. Method Application to Spanish Peaks

To evaluate mesoscale structures in the HT space, we use the Spanish Peaks data set as a clear example of diverse structures. The two radial structures and linear dikes overlap in Cartesian space but form distinct bands in HS (Figure 8). We apply the radial swarm equation to the Spanish Peaks data set to find the center of the radial structures. First, we segment the data using Northing value of the segment midpoint into two sections ($Y > 4{,}520{,}000$ and $4{,}480{,}000\text{ m} < Y < 4{,}520{,}000$ m) then fit Equation 8 with a radius ($R_{\max}$) of 2.5 km (see Figures 8a and 8b). We find two radial centers, one centered on West Peak (green, $R^2 = 0.75$) and another centered on Dike Mountain (purple, $R^2 = 0.93$). The distributions of angles in the radial swarm are mostly flat indicating even angular spacing except for slight increases around −55°–90° where some of the linear swarm dikes intersect with the radial swarm. For these specific dikes, it is ambiguous whether they should be counted as radial or linear. More data such as geochemistry or radiometric dating could help differentiate them.

7. What Multiscale Structure Exists in the CFB Data Sets?

7.1. Radial and Circumferential Patterns

The HT based analysis can be used to quantitatively test the dike meso-structure. Applying the methodology described above to find radial structures in the larger CFB data sets, we first attempt to fit the entire data sets for CRBG and DT respectively to Equation 8 to find a common origin for the entire data sets. This provides

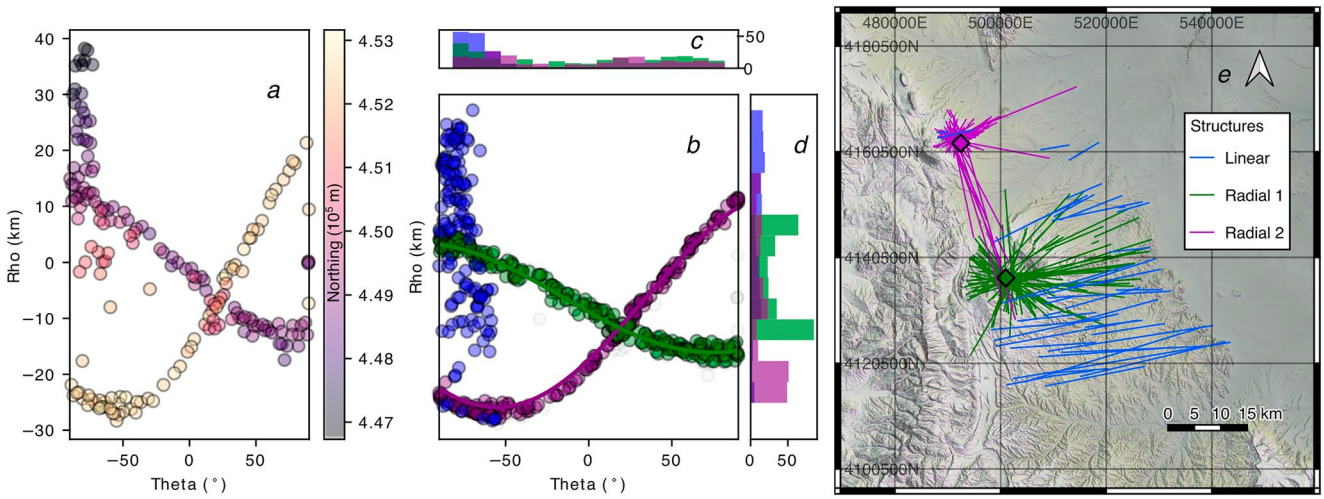

Figure 8. Analysis of the Spanish Peaks data set. (a) Hough space colored by the segment midpoint Northing. (b) Radial fits using Equation 8 and the segments which intersect within 2,500 km of the centers and the remaining linear structure in blue. (c and d) Shows the distribution of θ and ρ respectively for the linear, and two radial structures. (e) Clustered lines for the three identified structures in Cartesian coordinates. This figure can be replicated using the demo file in our linked Github repository.

a quantitative way to evaluate whether a single radial center fits the data sets, as has been suggested to result from impingement of an idealized radial plume head on the lithosphere (e.g., Buchan & Ernst, 2021; Ernst & Buchan, 1997). For both the CRBG and DT segment data sets (or linked data sets), we do not find a well fit radial center for the entirety of the data set ($R^2 = 0.005$ and 0.03 for CRBG and Deccan respectively, see Table 2). Thus, dike patterns, using a much larger data set than previous work, do not support a model wherein either an axisymmetric plume head or a single large magma reservoir controls the dike pattern. Likewise, a large circumferential swarm would show clearly in the data as two parallel sinusoids of ≈100–300 km apart. We do not observe these structures with our current data.

However, looking at subsets of the data sets, filtered based on segment midpoint Northing, we do find mesoscale radial patterns in both CFBs wherein all the dikes have intersections within a radius (R_{max}) of 10 km. In the CRBG data sets, we find two candidate radial patterns—one centered in the Wallowa mountains region at (469438E, 5001913N—UTM Zone 11N, EPSG 26911 projection) and a second radial center south of the highest density of dike exposure in the CJDS (472343E, 4933589N). This second potential center (red in Figure 9e) lies the within proposed centralized magma storage of Wolff et al. (2008). In the CRBG, the magma chamber south of the Wallowa mountains has been proposed by previous studies based on a geochemical analysis (Wolff et al., 2008). This potential magma source could explain the southern-most radial center found via the HT and

Table 2
Radial Center Fits

Data set	Center location (UTM)	R^2	Segments within ±10 km	Visualization
Spanish Peaks	[−11687300 4491720]	0.75	236	Green Figure 8
	[−11698060 4523900]	0.93	217	Purple Figure 8
CRBG:CJDS	[469240 4980220]	0.00	Whole data set Fit	White Diamond Figure 9e
	[472340 49335890]	0.14	766	Red Figure 9e
	[469440 5001910]	0.25	1,578	Green Figure 9e
Deccan	[8103600 2420780]	0.03	Whole data set Fit	White Diamond Figure 9f
	[8121290 2141440]	0.81	650	Red Figure 9f
	[7919540 2394060]	0.91	3,607	Green Figure 9f
	[9080900 2698270]	0.97	454	Purple Figure 9f
	[8224210 1813000]	0.99	234	Yellow Figure 9f

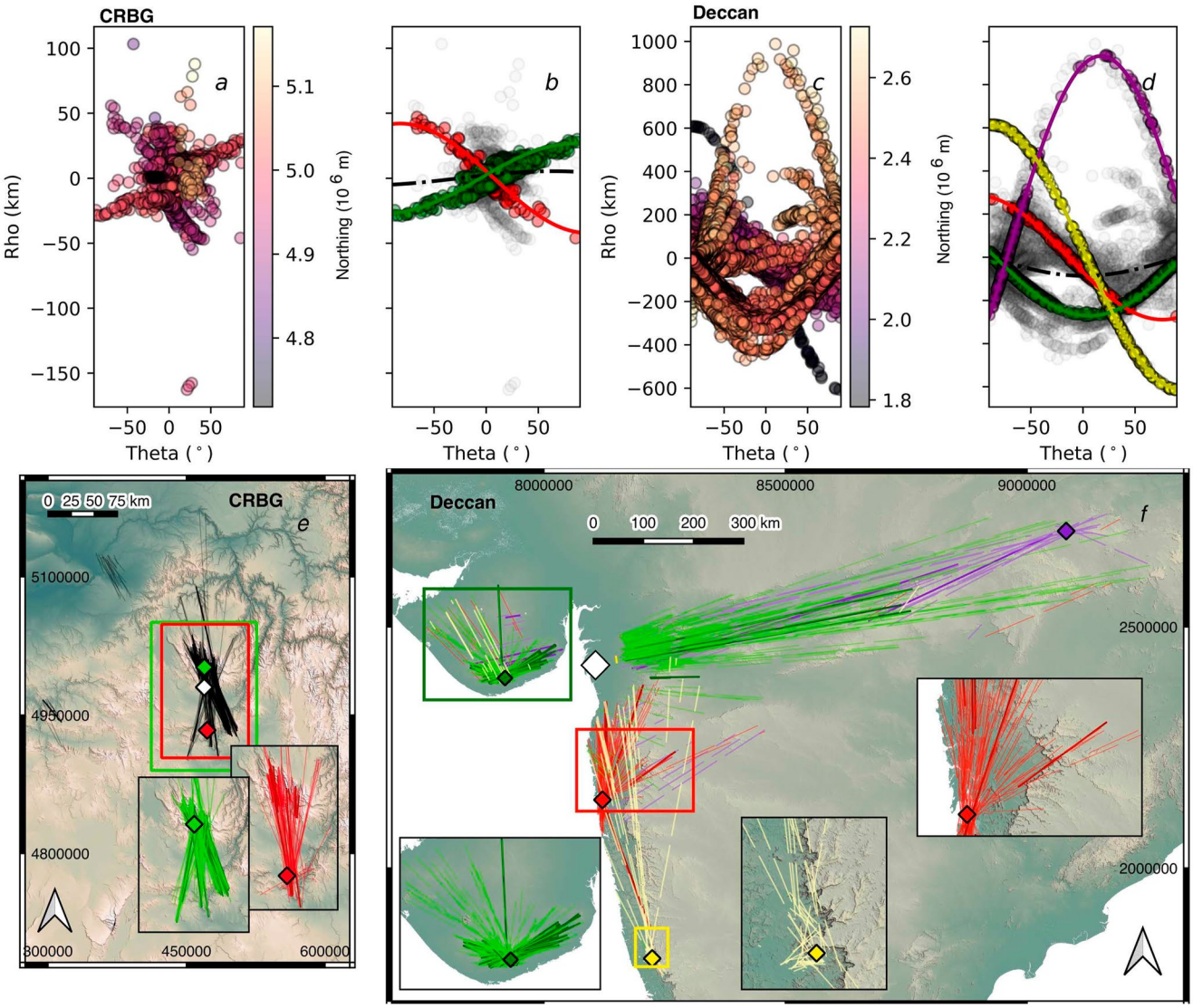

Figure 9. (a and c) Shows the Hough Space colored by the cluster midpoint Northing for the Columbia River Flood Basalt Group and Deccan respectively. (b and d) Shows possible radial fits using Equation 8. (e and f) Shows all clusters which fall within a 10 km radius of each radial center while the bold lines show the filtered lines which fall within this radius. White diamonds show in (e and f) show the locations of the best fit radial center for the whole data set. Zoomed in panels of each inset with the radial centers and segments that fit them can be found in Supporting Information S1. Exact locations of centers available in Table 2.

aligns roughly with the inferred centroid of dilation in Figure 6a. However, the goodness of fit for these structures is however low (R_{sq} = 0.26, 0.15 respectively). A more complex HS pattern may provide a better fit to the dike segment distribution but it's unclear what these complex patterns might mean for the stress conditions. Further work could be done to incorporate HS patterns and crustal stress modeling. We cannot rule out the possibility that apparent radial patterns in the CJDS simply arise from overlapping linear features with variable orientation. We believe that these apparent radial dike patterns in both CFBs warrant further study. However, the robustness of this structure is not very significant.

In the Deccan database, we find several possible radial structures with significantly better goodness of fits than what is seen in the CRBG. First, we find a center (Figure 9f, green) centered in the Saurashtra subswarm (7919544E, 2394058N—Pseudo-Mercator, EPSG 3857) with goodness of fit of R_{sq} = 0.91 and 3,600 dikes which intersect with this proposed center. Notably, this structure extends well into the Narmada-Tapi rift zone which is strongly linear and is 100s of kilometers away. The fits do not account for Cartesian endpoints of the segments or clusters. The second best fit center is centered near Mumbai at 8121286E, 2141444N (Figures 7A–7E, red) with goodness of fit of R_{sq} = 0.81. We show two other possible centers (Figures 7A–7E, purple and yellow) with high

goodness of fit (R_{sq} = 0.97 and 0.99). However due their large distance from the HT origin of the data set, we are unsure whether these swarms associations are physical (Figure 9f yellow inset). Looking at them in the Cartesian space, they do not appear as radiating fans which leads us to think that these linkages may be artifacts of HT distortion which occur due to the extremely large area over which the HT is taking place. Although the radial structures are more clear for the Deccan Traps, there is no clear geological or geophysical evidence of a localized magma reservoir associated with the center of the radial dike swarms to date (Dole et al., 2022; Rajaram et al., 2017; Rao et al., 2022; Self et al., 2022b). The radial patterns we observe may instead represent a time evolving stress state in which successive linear trends are emplaced with changes in angle such as in Figure 7b. Additional data is necessary to evaluate and assign physical interpretation to these structures. Our results thus provide useful targets for future targeted work that can help address important questions related to the magmatic architecture of CFBs.

7.2. Linear Trends

We consider a linear swarm to be defined by a set of subparallel dikes oriented along an axis. A linear swarm has a length and width in Cartesian space that correspond to a range of angles and ρs in HS. A narrow range in angles is essential. To identify orientations with linear activity we examine the histogram of the HS and look for concentrations of dikes within narrow bins of θ and ρ in a method analogous to the traditional use of the HT accumulator array (Figure 10). Looking at the bins with the highest counts, we can establish packets of linearly oriented dikes. The top three bins of the HT histogram for CRBG and Deccan represent 11% and 12% of all segments respectively. In the CRBG, this represents a range of only 14° and each bin is adjacent to the others since it is strongly linear. In the Deccan, the top three bins represent a range of 21°.

In the Deccan, the major linear trends are in the Narmada-Tapi rift zone between −85° and −65° and extend for well over 100 km and slightly into the Saurashtra region (Figure 10). These overlap with the radial swarms found above and can also be part of the radial swarm fits. The identification of dikes as being part of both a linear and radial structure gives interesting information about the structure. This may be indicative of the fact that the presence of a slowly rotating stress field leads to the formation of multiple linear type structures. These in turn overlap and forming a fanning structure (similar to what is shown in Figure 7B) rather than a true radial structure. In CRBG, we find two subparallel axes of linear dikes structure with high dike concentrations. These structures connect areas of high dike density which appear in the granites associated with the Wallowa mountains and isolated granite stocks to the south (Morriss et al., 2020; Petcovic & Grunder, 2003).

8. Comparing Deccan and Columbia River Flood Basalts

The Deccan Traps erupted volume is at least 6*x* greater than the CRBG in eruptive volume (1,300,000 km^3 vs. 210,000 km^3, Figure 11) (Jay & Widdowson, 2008; Kasbohm & Schoene, 2018). Is this volumetric difference in erupted volume reflected in the shallow crustal dike swarm exposures? Most magma never erupts at the surface, so directly linking exposed dikes to eruptive volume in general is difficult (Gudmundsson, 2002; Townsend & Huber, 2020). Nevertheless, the large scale of upper crustal dike swarms as analyzed in this study provides a unique opportunity for comparison. First, the Deccan dike segment database (n = 25, 938) is larger than the CRBG (n = 4,340) by a factor of 5.9, similar to the erupted volume ratio. Although there are significantly different observational biases, especially due to different exposures, in the CRBG and DT data sets we do posit that the difference in dike segment numbers scales with the erupted volume. In the unfiltered clustered database the ratio (DT to CRBG) is also approximately maintained at 5.2*x*. The filtered database ratio is 13*x*, but is less directly comparable due to the different ρ threshold for the Deccan swarm.

The median length of Deccan clusters as shown by the HT (~93 km) is significantly longer (3*x*) than the CRBG clusters (~29 km). Comparing the ratio of eruptive volume to median length we see similar ratios of 11 and 7 square kilometers. The median width of Deccan clusters (~2 km) is larger than the CRBG clusters (~0.7 km). Although this difference might be attributed to the ρ thresholds based on segment mean length between the CFBs, we note that similar widths arise if a comparable ρ threshold had been used for the CRBG (see Supporting Information S1). The median cluster aspect ratios are similar 53 versus 48 for the Deccan and CRBG respectively (Figure 8d). The similar cluster aspect ratios implies that the dike emplacement mechanics are the same for both swarms despite the significantly longer clustered dikes in the Deccan. Individual dike aspect ratios are predicted using LEFM however what we show are dike clusters also show similar aspect ratios implying that dike swarming mechanisms in both systems are similar. This could support the idea that the eruptions are fed by distributed magma reservoirs. Finally, the amount of estimated maximum dilational strain is similar for both swarms despite their difference in spatial area.

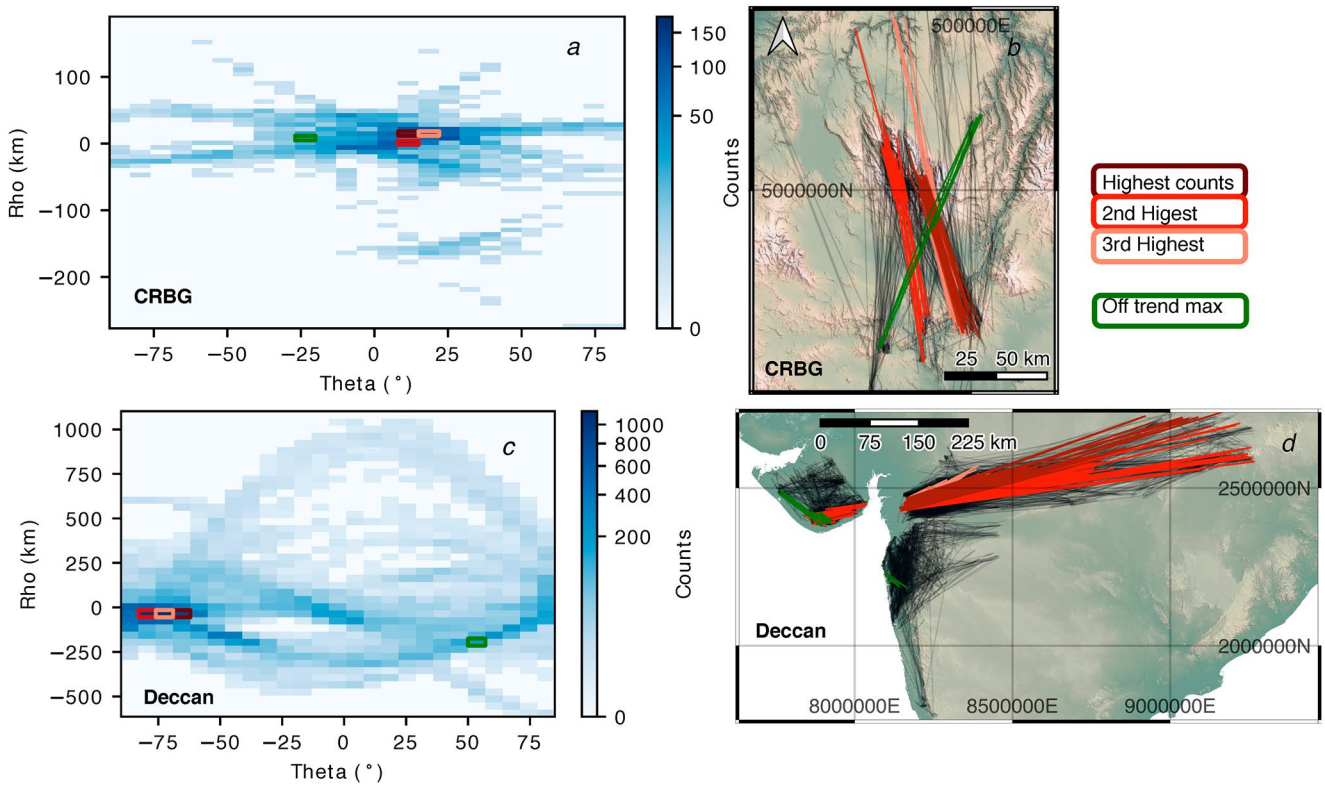

Figure 10. (a and c) Shows a histogram of the Hough transform segment database as a function of ρ and θ with dark blue colors indicating higher counts in that orientation. The bins of the histogram are set to be a width of 7° in angle and 2.5% of the range of ρ. (b and d) Shows the top three bins of the histogram (maroon, red, and pink) in Cartesian space along with an off-axis maximum shown in green. The off axis maximum is the highest bin more than 50° away from the main linear trend (red box). We use the segment orientations for the histograms but show the linked dikes for ease of viewing.

Together, these similarities between clustered dike segments, in the context of erupted volume ratios between CRBG and Deccan, suggest that spatial patterns of CFB magmatic geometry scales with total eruptive output. Such structural similarities, measured both on province scale and via dike cluster sizes, are remarkable. Although two examples is hardly a robust trend, the implications are interesting and unexpected given significant differences in other aspects of the CFBs. We can also roughly extend this to the Spanish Peaks although the different geologic setting and unknown volumes make direct comparisons difficult. We use the swarm centered on West Peak, which may represent the scale of a typical long-lived volcanic center and paleo-edifice (Harp, 2021), to examine the scaling between area and number of dikes to CFBs. We use an estimated "erupted" volume for West Peak based on averages of volcanic complexes compiled in O'Hara et al. (2020) and Grosse et al. (2009). Extending the scaling trend to West Peak over estimates the erupted volume and area by up to two orders of magnitude however the comparison between the West Peak an the voluminous LIP data sets is difficult to make especially considering the high uncertainty on the West Peak eruptive system.

If erupted volumes are imprinted on the spatial structure of the transcrustal magma transport system, this scaling provides a tool for connecting surface volcanic expression to deep transport that is hidden from view. Conversely, it is also of interest to connect exhumed transport systems such as Spanish Peaks, plutonic systems (Karlstrom et al., 2017), and ancient dike swarms (Baragar et al., 1996; Fahrig & Jones, 1969), or planetary examples (Ernst et al., 1995), to their surface expressions.

9. Conclusion

We have developed a tool based on the HT for objective extraction of structures in complex distributions of quasi-linear segments, such as are prevalent in terrestrial dike swarms. We have tested this tool with synthetic data and applied it to three dike swarms, associated with the Spanish Peaks, Colorado, USA, the Columbia River Flood Basalts, USA, and the Deccan Traps, India. We found that dike segments can be linked together

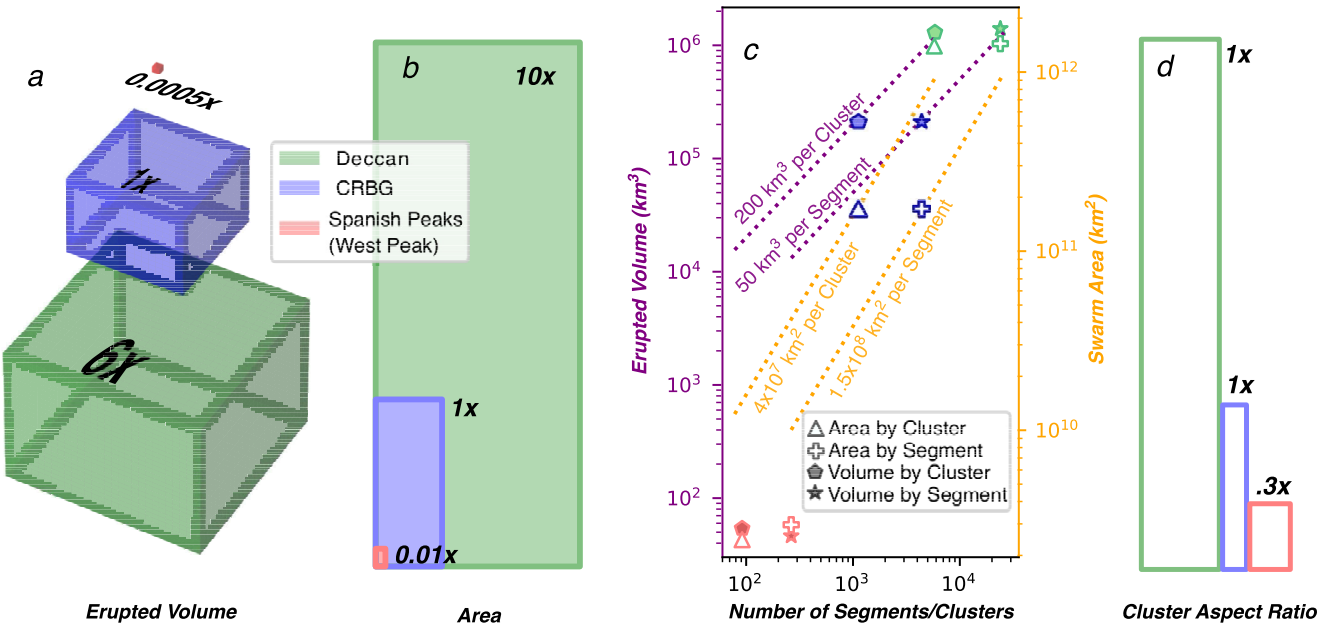

Figure 11. (a) Comparison of the erupted volume of Deccan Traps, Columbia River Flood Basalt Group, and Spanish Peaks specifically the West Peak on which the radial swarm is centered (Jay & Widdowson, 2008; Kasbohm & Schoene, 2018; Reidel, Camp, Tolan, & Martin, 2013). Since there are no extrusive deposits associated with Spanish Peaks, the West Peak erupted volume is estimated based on (Grosse et al., 2009) assuming an intrusive extrusive ratio of at least 1:2 and is used as a rough example of one eruptive center. (b) Compares the swarm areas. (c) Plots the number of dikes or clusters versus the erupted volume (left, purple, filled symbols) and the swarm area (right, orange, white symbols) for the three dike swarms. We have also plotted estimated lines of the erupted volume and area per segment and cluster which is roughly constant for the limited data. (d) Shows the relative dike cluster widths and lengths and is annotated with the ratios of dike cluster aspects which again are roughly constant for the three examples.

into aligned structures that may represent dikes or packets of highly clustered dikes. Looking at the linked data sets we find significantly longer sustained structures which average 30 km in CFBs and can reach over 200 km. The HT also facilitates investigation of dike swarm mesoscale structure in two end members: linear and radial patterns. First, we do not find that a single radial or circumferential center is well fit by the dike data in any of the three provinces. However, we do find that the dike swarms can be decomposed into smaller localized radial patterns which may represent rotating stress fields over time or the influence of an isotropic stress field.

For CFBs, the apparent generality of structures and scaling provide a template for future study both of the CRBG and Deccan as well as other flood basalt systems. We expect that future work incorporating compositions (Reidel, Camp, Tolan, & Martin, 2013), paleomagnetic polarity (Biasi & Karlstrom, 2021), and direct geochronology (Fendley et al., 2019; Kasbohm & Schoene, 2018; Schoene et al., 2021; Sheth et al., 2019) will be necessary to robustly link individual segments together. Additional statistical characterization, such as analysis of the dendrogram generated via the hierarchical clustering methods (Jarman, 2020), could seek to establish the range of mesoscale structures that exist. Additionally, the HT method could be generalized to include curvilinear segments, which are not uncommon in dike swarms but neglected here for simplicity. This method as described here which we applied to dike swarms could also be applied to many types of linear/curved structures including fracture sets, fault networks, and shear zones on Earth or on other planets.

Data Availability Statement

The data sets generated by our linking method and the digitized, unprocessed Spanish Peaks data set are available in Supporting Information S1 and at (Hutchison et al., 2023). The code used to create those data sets and figures in the paper are available for inspection and citation at (Hutchison, 2022). The code includes a demonstration file which can be run to replicate our Spanish Peaks results and learn about the algorithm.

Acknowledgments
The authors thank Chris Harper for his insightful discussion in developing this method and the 2020 and 2021 Columbia River Flood Basalts reading group organized by Leif Karlstrom with special thanks to Emily Cahoon, Dylan Patrick Colon, Maria McQuillan, and Mary Mass who were part of the initial work on this project. Thank you to Richard Ernst and an anonymous reviewer for their comments and suggestions which improved this manuscript. TM acknowledges support by the MIT Crosby Postdoctoral Fellowship. LK acknowledges NSF Grant 1848554.

References

Acocella, V., & Neri, M. (2009). Dike propagation in volcanic edifices: Overview and possible developments. *Tectonophysics*, *471*(1–2), 67–77. https://doi.org/10.1016/j.tecto.2008.10.002

Ayele, A., Jacques, E., Kassim, M., Kidane, T., Omar, A., Tait, S., et al. (2007). The volcano-seismic crisis in Afar, Ethiopia, starting September 2005. *Earth and Planetary Science Letters*, *255*(1–2), 177–187. https://doi.org/10.1016/j.epsl.2006.12.014

Babiker, M., & Gudmundsson, A. (2004). Geometry, structure and emplacement of mafic dykes in the Red Sea Hills, Sudan. *Journal of African Earth Sciences*, *38*(3), 279–292. https://doi.org/10.1016/j.jafrearsci.2004.01.003

Ballard, D. H. (1981). Generalizing the Hough transform to detect arbitrary shapes. *Pattern Recognition*, *13*(2), 111–122. https://doi.org/10.1016/0031-3203(81)90009-1

Baragar, W. R., Ernst, R. E., Hulbert, L., & Peterson, T. (1996). Longitudinal petrochemical variation in the Mackenzie dyke swarm, Northwestern Canadian Shield. *Journal of Petrology*, *37*(2), 317–359. https://doi.org/10.1093/petrology/37.2.317

Bhattacharji, S., Chatterjee, N., Wampler, J. M., Nayak, P. N., & Deshmukh, S. S. (1996). Indian intraplate and continental margin rifting, lithospheric extension, and mantle upwelling in Deccan flood basalt volcanism near the K/T boundary: Evidence from mafic dike swarms. *The Journal of Geology*, *104*(4), 379–398. https://doi.org/10.1086/629835

Biasi, J., & Karlstrom, L. (2021). Timescales of magma transport in the Columbia River flood basalts, determined by paleomagnetic data. *Earth and Planetary Science Letters*, *576*, 117169. https://doi.org/10.1016/j.epsl.2021.117169

Black, B. A., Karlstrom, L., & Mather, T. A. (2021). The life cycle of large igneous provinces. *Nature Reviews Earth & Environment*, *2*(12), 840–857. https://doi.org/10.1038/s43017-021-00221-4

Blakely, R. J., Sherrod, B. L., Weaver, C. S., Wells, R. E., & Rohay, A. C. (2014). The Wallula fault and tectonic framework of south-central Washington, as interpreted from magnetic and gravity anomalies. *Tectonophysics*, *624–625*, 32–45. https://doi.org/10.1016/j.tecto.2013.11.006

Bond, D. P., & Wignall, P. B. (2014). Large igneous provinces and mass extinctions: An update. *Special Paper of the Geological Society of America*, *505*, 29–55. https://doi.org/10.1130/2014.2505(02)

Buchan, K. L., & Ernst, R. E. (2021). *Plumbing systems of large igneous provinces (LIPs) on Earth and Venus: Investigating the role of giant circumferential and radiating dyke swarms, coronae and novae, and mid-crustal intrusive complexes*. (Vol. 100). Elsevier. https://doi.org/10.1016/j.gr.2021.02.014

Bunger, A. P., Menand, T., Cruden, A., Zhang, X., & Halls, H. (2013). Analytical predictions for a natural spacing within dyke swarms. *Earth and Planetary Science Letters*, *375*, 270–279. https://doi.org/10.1016/j.epsl.2013.05.044

Bunger, A. P., Zhang, X., & Jeffrey, R. G. (2012). Parameters affecting the interaction among closely spaced hydraulic fractures. *SPE Journal*, *17*(1), 292–306. https://doi.org/10.2118/140426-PA

Cahoon, E. B., Streck, M. J., Koppers, A. A., & Miggins, D. P. (2020). Reshuffling the Columbia River Basalt chronology—Picture gorge basalt, the earliest-and longest-erupting formation. *Geology*, *48*(4), 348–352. https://doi.org/10.1130/g47122.1

Callot, J. P., Geoffroy, L., Aubourg, C., Pozzi, J. P., & Mege, D. (2001). Magma flow directions of shallow dykes from the East Greenland volcanic margin inferred from magnetic fabric studies. *Tectonophysics*, *335*(3–4), 313–329. https://doi.org/10.1016/S0040-1951(01)00060-9

Camp, V. E., Reidel, S. P., Ross, M. E., Brown, R. J., & Self, S. (2017). Field-trip guide to the vents, dikes, stratigraphy, and structure of the Columbia River Basalt Group, eastern Oregon and southeastern Washington. Scientific Investigations Report 2017-5022-N. 88. https://doi.org/10.3133/sir20175022N

Camp, V. E., & Ross, M. E. (2004). Mantle dynamics and genesis of mafic magmatism in the intermontane Pacific Northwest. *Journal of Geophysical Research*, *109*(8), 1–14. https://doi.org/10.1029/2003JB002838

Crane, K., & Bohanon, A. (2021). Dike propagation during global contraction: Making sense of conflicting stress histories on Mercury. *Frontiers in Earth Science*, *9*, 1–14. https://doi.org/10.3389/feart.2021.752864

Davis, T., Bagnardi, M., Lundgren, P., & Rivalta, E. (2021). Extreme curvature of shallow magma pathways controlled by competing stresses: Insights from the 2018 Sierra Negra eruption. *Geophysical Research Letters*, *48*(13), 1–10. https://doi.org/10.1029/2021GL093038

Delaney, P. T., Pollard, D. D., Ziony, J. I., & McKee, E. H. (1986). Field relations between dikes and joints: Emplacement processes and paleostress analysis. *Journal of Geophysical Research*, *91*(B5), 4920. https://doi.org/10.1029/jb091ib05p04920

Dole, G., Das, S., & Kale, V. S. (2022). Tectonic framework of geomorphic evolution of the Deccan volcanic province, India. *Earth-Science Reviews*, *228*, 103988. https://doi.org/10.1016/j.earscirev.2022.103988

Duda, R. O., & Hart, P. E. (1972). Use of the Hough transformation to detect lines and curves in pictures. *Communications of the ACM*, *15*(1), 11–15. https://doi.org/10.1145/361237.361242

Eberhardt, E. (2012). The Hoek–Brown failure criterion. In *The ISRM suggested methods for rock characterization, testing and monitoring: 2007-2014* (pp. 233–240). Springer.

Ernst, R. E., Bond, D. P. G., Zhang, S., Buchan, K. L., Grasby, S. E., Youbi, N., et al. (2021). Large igneous province record through time and implications for secular environmental changes and geological time-scale boundaries (pp. 1–26). https://doi.org/10.1002/9781119507444.ch1

Ernst, R. E., & Buchan, K. L. (1997). Giant radiating dyke swarms: Their use in identifying pre-Mesozoic large igneous provinces and mantle plumes. *Geophysical Monograph Series*, *100*, 297–333. https://doi.org/10.1029/GM100p0297

Ernst, R. E., Grosfils, E. B., & Mege, D. (2001). Giant dike swarms: Earth, Venus, and Mars. *Annual Review of Earth and Planetary Sciences*, *29*(29), 489–534. https://doi.org/10.1146/annurev.earth.29.1.489

Ernst, R. E., Head, J. W., Parfitt, E., Grosfils, E., & Wilson, L. (1995). Giant radiating dyke swarms on Earth and Venus. *Earth-Science Reviews*, *39*(1–2), 1–58. https://doi.org/10.1016/0012-8252(95)00017-5

Everitt, B. (1980). Cluster analysis. *14*(1), 75–100. https://doi.org/10.1007/BF00154794

Fahrig, W. F., & Jones, D. L. (1969). Paleomagnetic evidence for the extent of Mackenzie igneous events. *Canadian Journal of Earth Sciences*, *6*(4), 679–688. https://doi.org/10.1139/e69-065

Fendley, I. M., Mittal, T., Sprain, C. J., Marvin-DiPasquale, M., Tobin, T. S., & Renne, P. R. (2019). Constraints on the volume and rate of Deccan Traps flood basalt eruptions using a combination of high-resolution terrestrial mercury records and geochemical box models. *Earth and Planetary Science Letters*, *524*, 115721. https://doi.org/10.1016/j.epsl.2019.115721

Fruchter, J. S., & Baldwin, S. F. (1975). Correlations between dikes of the monument swarm, central Oregon, and picture gorge basalt flows. *Geological Society of America Bulletin*, *86*(4), 514–516. https://doi.org/10.1130/0016-7606(1975)86<514:cbdotm>2.0.co;2

Glazner, A. F., & Mills, R. D. (2012). Interpreting two-dimensional cuts through broken geologic objects: Fractal and non-fractal size distributions. *Geosphere*, *8*(4), 902–914. https://doi.org/10.1130/GES00731.1

Glen, J. M. G., & Ponce, D. A. (2002). Large-scale fractures related to inception of the Yellowstone hotspot. *Geology*, *30*(7), 647–650. https://doi.org/10.1130/0091-7613(2002)030⟨0647:LSFRTI⟩2.0.CO;2

Gonnermann, H., & Taisne, B. (2015). Magma transport in dikes author's personal copy. *Encyclopedia of Volcanoes*, 215–224.

Grosfils, E. B., & Head, J. W. (1994). Emplacement of a radiating dike swarm in western Vinmara Planitia, Venus: Interpretation of the regional stress field orientation and subsurface magmatic configuration.
Grosse, P., van Wyk de Vries, B., Petrinovic, I. A., Euillades, P. A., & Alvarado, G. E. (2009). Morphometry and evolution of arc volcanoes. *Geology*, *37*(7), 651–654. https://doi.org/10.1130/G25734A.1
GSI Bhukosh. (2020). Bhukosh. [Computer software manual]. Retrieved from http://bhukosh.gsi.gov.in/
GSI District Resource Map. (2001). District resource maps—India (Technical Report).
Gudmundsson, A. (1995). Infrastructure and mechanics of volcanic systems in Iceland. *Journal of Volcanology and Geothermal Research*, *64*(1–2), 1–22. https://doi.org/10.1016/0377-0273(95)92782-Q
Gudmundsson, A. (2002). Emplacement and arrest of sheets and dykes in central volcanoes. *Journal of Volcanology and Geothermal Research*, *116*(3–4), 279–298. https://doi.org/10.1016/S0377-0273(02)00226-3
Gudmundsson, A. (2006). How local stresses control magma-chamber ruptures, dyke injections, and eruptions in composite volcanoes. *Earth-Science Reviews*, *79*(1–2), 1–31. https://doi.org/10.1016/j.earscirev.2006.06.006
Gunaydin, D., Peirce, A. P., & Bunger, A. P. (2021). Laboratory experiments contrasting growth of uniformly and nonuniformly spaced hydraulic fractures. *Journal of Geophysical Research: Solid Earth*, *126*(1), e2020JB020107. https://doi.org/10.1029/2020JB020107
Harp, A. G. (2021). Magma propagation and emplacement within the central intrusive complex of Summer Coon stratovolcano, Colorado. *Journal of Volcanology and Geothermal Research*, *419*, 107372. https://doi.org/10.1016/j.jvolgeores.2021.107372
Hough, P. V. C. (1962). A method and means for recognition complex patterns.
Hutchison, A. K. (2022). *aikubo/linking-and-clustering-dikes: v0.1.1-review*. Zenodo. https://doi.org/10.5281/zenodo.7415877
Hutchison, A. K., Karlstrom, L., & Mittal, T. (2023). *Multiscale spatial patterns in giant dike swarms identified through objective feature extraction datasets*. Zenodo. https://doi.org/10.5281/zenodo.8007348
Jarman, A. M. (2020). Hierarchical cluster analysis: Comparison of single linkage, complete linkage, average linkage and centroid linkage method. (pp. 1–13). Retrieved from https://www.researchgate.net/publication/339443595_Hierarchical_Cluster_Analysis_Comparison_of_Single_linkageComplete_linkage_Average_linkage_and_Centroid_Linkage_Method
Jay, A. E., & Widdowson, M. (2008). Stratigraphy, structure and volcanology of the SE Deccan continental flood basalt province: Implications for eruptive extent and volumes. *Journal of the Geological Society*, *165*(1), 177–188. https://doi.org/10.1144/0016-76492006-062
John, D. U. G. S., Wallace, A. U. G. S., Ponce, D., Fleck, R., & Conrad, J. (2000). New perspectives on the geology and origin of the northern Nevada rift.
Johnson, R. (1961). Patterns and origin of radial dike swarms associated with West Spanish peak and Dike Mountain, South-Central Colorado. *Geological Society of America Bulletin*, *72*, 579–590. https://doi.org/10.1130/0016-7606(1961)72[579:paoord]2.0.co;2
Jolly, R. J., & Sanderson, D. J. (1995). Variation in the form and distribution of dykes in the Mull swarm, Scotland. *Journal of Structural Geology*, *17*(11), 1543–1557. https://doi.org/10.1016/0191-8141(95)00046-G
Karlstrom, L., Dufek, J., & Manga, M. (2009). Organization of volcanic plumbing through magmatic lensing by magma chambers and volcanic loads. *Journal of Geophysical Research*, *114*(10), 1–16. https://doi.org/10.1029/2009JB006339
Karlstrom, L., Paterson, S. R., & Jellinek, A. M. (2017). A reverse energy cascade for crustal magma transport. *Nature Geoscience*, *10*(8), 604–608. https://doi.org/10.1038/NGEO2982
Kasbohm, J., & Schoene, B. (2018). Rapid eruption of the Columbia River flood basalt and correlation with the mid-Miocene climate optimum. *Science Advances*, *4*(9), 8223. Retrieved from https://www.science.org/doi/10.1126/sciadv.aat8223
Kavanagh, J. L., & Pavier, M. (2014). Rock interface strength influences fluid-filled fracture propagation pathways in the crust. *Journal of Structural Geology*, *63*, 68–75. https://doi.org/10.1016/j.jsg.2014.03.001
Kavanagh, J. L., Boutelier, D., & Cruden, A. R. (2015). The mechanics of sill inception, propagation and growth: Experimental evidence for rapid reduction in magmatic overpressure. *Earth and Planetary Science Letters*, *421*, 117–128. https://doi.org/10.1016/j.epsl.2015.03.038
Kavanagh, J. L., Burns, A. J., Hilmi Hazim, S., Wood, E. P., Martin, S. A., Hignett, S., & Dennis, D. J. (2018). Challenging dyke ascent models using novel laboratory experiments: Implications for reinterpreting evidence of magma ascent and volcanism. *Journal of Volcanology and Geothermal Research*, *354*, 87–101. https://doi.org/10.1016/j.jvolgeores.2018.01.002
Kavanagh, J. L., Menand, T., & Sparks, R. S. J. (2006). An experimental investigation of sill formation and propagation in layered elastic media. *Earth and Planetary Science Letters*, *245*(3–4), 799–813. https://doi.org/10.1016/j.epsl.2006.03.025
Krumbholz, M., Hieronymus, C. F., Burchardt, S., Troll, V. R., Tanner, D. C., & Friese, N. (2014). Weibull-distributed dyke thickness reflects probabilistic character of host-rock strength. *Nature Communications*, *5*, 1–7. https://doi.org/10.1038/ncomms4272
Ma, L., Li, Z., Wang, M., Wu, J., & Li, G. (2020). Applicability of a new modified explicit three-dimensional Hoek-Brown failure criterion to eight rocks. *International Journal of Rock Mechanics and Mining Sciences*, *133*, 104311. https://doi.org/10.1016/j.ijrmms.2020.104311
Mège, D., & Korme, T. (2004). Dyke swarm emplacement in the Ethiopian Large Igneous Province: Not only a matter of stress. *Journal of Volcanology and Geothermal Research*, *132*(4), 283–310. https://doi.org/10.1016/S0377-0273(03)00318-4
Mittal, T., & Richards, M. A. (2021). The magmatic architecture of continental flood basalts: 2. A new conceptual model. *Journal of Geophysical Research: Solid Earth*, *126*(12), e2021JB021807. https://doi.org/10.1029/2021JB021807
Mittal, T., Richards, M. A., & Fendley, I. M. (2021). The magmatic architecture of continental flood basalts I: Observations from the Deccan Traps. *Journal of Geophysical Research: Solid Earth*, *126*(12), 1–81. https://doi.org/10.1029/2021jb021808
Morriss, M. C., Karlstrom, L., Nasholds, M. W., & Wolff, J. A. (2020). The chief Joseph dike swarm of the Columbia River flood basalts, and the legacy data set of William H. Taubeneck. *Geosphere*, *16*(4), 1793–1817. https://doi.org/10.1130/GES02173.1
Muller, O. H., & Pollard, D. D. (1977). The stress state near Spanish Peaks, Colorado determined from a dike pattern. *Pure and Applied Geophysics PAGEOPH*, *115*(1–2), 69–86. https://doi.org/10.1007/BF01637098
Müllner, D. (2011). Modern hierarchical, agglomerative clustering algorithms. (1973). (pp. 1–29). Retrieved from http://arxiv.org/abs/1109.2378
Nicolas, A., Boudier, F., Koepke, J., France, L., Ildefonse, B., & Mevel, C. (2008). Root zone of the sheeted dike complex in the Oman ophiolite. *Geochemistry, Geophysics, Geosystems*, *9*(5), Q05001. https://doi.org/10.1029/2007gc001918
Odé, H. (1957). Mechanical analysis of the dike pattern of the Spanish Peaks area, Colorado. *Bulletin of the Geological Society of America*, *68*(5), 567–576. https://doi.org/10.1130/0016-7606(1957)68[567:MAOTDP]2.0.CO;2
O'Hara, D., Karlstrom, L., & Ramsey, D. W. (2020). Time-evolving surface and subsurface signatures of Quaternary volcanism in the Cascades arc. *Geology*, *48*(11), 1088–1093. https://doi.org/10.1130/G47706.1
Paquet, F., Dauteuil, O., Hallot, E., & Moreau, F. (2007). Tectonics and magma dynamics coupling in a dyke swarm of Iceland. *Journal of Structural Geology*, *29*(9), 1477–1493. https://doi.org/10.1016/j.jsg.2007.06.001
Penn, B. S., & Lindsey, D. A. (2009). $^{40}Ar/^{39}Ar$ dates for the Spanish Peaks intrusions in south-central Colorado. *Rocky Mountain Geology*, *44*(1), 17–32. https://doi.org/10.2113/gsrocky.44.1.17

Petcovic, H. L., & Grunder, A. (2003). Textural and thermal history of partial melting in tonalitic wallrock at the margin of a basalt dike, Wallowa Mountains, Oregon. *Journal of Petrology*, *44*(12), 2287–2312. https://doi.org/10.1093/petrology/egg078

Petcovic, H. L., & Dufek, J. D. (2005). Modeling magma flow and cooling in dikes: Implications for emplacement of Columbia River flood basalts. *Journal of Geophysical Research*, *110*(10), 1–15. https://doi.org/10.1029/2004JB003432

Pollard, D. D., Segall, P., & Delaney, P. T. (1982). Formation and interpretation of dilatant echelon cracks. *Geological Society of America Bulletin*, *93*(12), 1291–1303. https://doi.org/10.1130/0016-7606(1982)93⟨1291:FAIODE⟩2.0.CO;2

Rajaram, M., Anand, S., Erram, V. C., & Shinde, B. (2017). Insight into the structures below the Deccan trap-covered region of Maharashtra, India from geopotential data. *Geological Society, London, Special Publications*, *445*(1), 219–236. https://doi.org/10.1144/sp445.8

Rao, J., Ravikumar, B., & Golani, P. R. (2022). What lies beneath the Deccan volcanic province? Perspective on tectonic elements and sub-trappean geology from gravity signatures. *Journal of Earth System Science*, *131*(1), 1–20. https://doi.org/10.1007/s12040-021-01787-9

Ray, R., Sheth, H. C., & Mallik, J. (2007). Structure and emplacement of the Nandurbar-Dhule mafic dyke swarm, Deccan Traps, and the tectonomagmatic evolution of flood basalts. *Bulletin of Volcanology*, *69*(5), 537–551. https://doi.org/10.1007/s00445-006-0089-y

Reidel, S. P., Camp, V. E., Tolan, T. L., Kauffman, J. D., & Garwood, D. L. (2013). Tectonic evolution of the Columbia River flood basalt province. *Special Paper of the Geological Society of America*, *497*, 293–324. https://doi.org/10.1130/2013.2497(12)

Reidel, S. P., Camp, V. E., Tolan, T. L., & Martin, B. S. (2013). *The Columbia River flood basalt province: Stratigraphy, areal extent, volume, and physical volcanology* (Vol. 497, pp. 1–43). Special Paper of the Geological Society of America. https://doi.org/10.1130/2013.2497(01)

Rivalta, E., Taisne, B., Bunger, A. P., & Katz, R. F. (2015). A review of mechanical models of dike propagation: Schools of thought, results and future directions. *Tectonophysics*, *638*(C), 1–42. https://doi.org/10.1016/j.tecto.2014.10.003

Rivas-Dorado, S., Ruíz, J., & Romeo, I. (2022). Giant dikes and dike-induced seismicity in a weak crust underneath Cerberus Fossae, Mars. *Earth and Planetary Science Letters*, *594*, 117692. https://doi.org/10.1016/J.EPSL.2022.117692

Roman, A., & Jaupart, C. (2014). The impact of a volcanic edifice on intrusive and eruptive activity. *Earth and Planetary Science Letters*, *408*, 1–8. https://doi.org/10.1016/j.epsl.2014.09.016

Rubin, A. M. (1995). Propagation of magma-filled cracks. *Annual Review of Earth and Planetary Sciences*, *23*(1), 287–336. https://doi.org/10.1146/annurev.ea.23.050195.001443

Schoene, B., Eddy, M. P., Keller, C. B., & Samperton, K. M. (2021). An evaluation of Deccan Traps eruption rates using geochronologic data. *Geochronology*, *3*(1), 181–198. https://doi.org/10.5194/gchron-3-181-2021

Self, S., Mittal, T., Dole, G., & Vanderkluysen, L. (2022a). Toward understanding Deccan volcanism. *Annual Review of Earth and Planetary Sciences*, *50*(1), 477–506. https://doi.org/10.1146/annurev-earth-012721-051416

Self, S., Mittal, T., Dole, G., & Vanderkluysen, L. (2022b). Toward understanding Deccan volcanism. *Annual Review of Earth and Planetary Sciences*, *50*(1), 477–506. https://doi.org/10.1146/annurev-earth-012721-051416

Sheth, H. C., Vanderkluysen, L., Demonterova, E. I., Ivanov, A. V., & Savatenkov, V. M. (2019). Geochemistry and $^{40}Ar/^{39}Ar$ geochronology of the Nandurbar-Dhule mafic dyke swarm: Dyke-sill-flow correlations and stratigraphic development across the Deccan flood basalt province. *Geological Journal*, *54*(1), 157–176. https://doi.org/10.1002/gj.3167

Sheth, H. C., & Cañón-Tapia, E. (2015). Are flood basalt eruptions monogenetic or polygenetic? *International Journal of Earth Sciences*, *104*(8), 2147–2162. https://doi.org/10.1007/s00531-014-1048-z

Shukla, G., Mallik, J., & Mondal, P. (2022). Dimension-scaling relationships of Pachmarhi dyke swarm and their implications on Deccan magma emplacement. *Tectonophysics*, *843*, 229602. https://doi.org/10.1016/J.TECTO.2022.229602

Sneath, P. H. (1957). The application of computers to taxonomy. *Journal of General Microbiology*, *17*(1), 201–226. https://doi.org/10.1099/00221287-17-1-201/CITE/REFWORKS

Sorenson, T. (1948). A method of establishing groups of equal amplitude in plant sociology based on similarity of species content and its application to analyses of the vegetation on Danish commons. *Biologiske Skrifter*, *5*, 1–34.

Thiele, S. T., Cruden, A. R., Micklethwaite, S., Bunger, A. P., & Köpping, J. (2020). Dyke apertures record stress accumulation during sustained volcanism. *Scientific Reports*, *10*(1), 1–9. https://doi.org/10.1038/s41598-020-74361-w

Townsend, M., & Huber, C. (2020). A critical magma chamber size for volcanic eruptions. *Geology*, *48*(5), 431–435. https://doi.org/10.1130/G47045.1

Urbani, S., Acocella, V., & Rivalta, E. (2018). What drives the lateral versus vertical propagation of dikes? Insights from analogue models. *Journal of Geophysical Research: Solid Earth*, *123*(5), 3680–3697. https://doi.org/10.1029/2017JB015376

Vanderkluysen, L., Mahoney, J. J., Hooper, P. R., Sheth, H. C., & Ray, R. (2011). The feeder system of the Deccan Traps (India): Insights from dike geochemistry. *Journal of Petrology*, *52*(2), 315–343. https://doi.org/10.1093/petrology/egq082

Virtanen, P., Gommers, R., Oliphant, T. E., Haberland, M., Reddy, T., Cournapeau, D., et al. (2020). SciPy 1.0: Fundamental algorithms for scientific computing in Python. *Nature Methods*, *17*(3), 261–272. https://doi.org/10.1038/s41592-019-0686-2

Wadge, G., Biggs, J., Lloyd, R., & Kendall, J. M. (2016). Historical volcanism and the state of stress in the east African rift system. *Frontiers in Earth Science*, *4*. https://doi.org/10.3389/feart.2016.00086

Wolff, J. A., Ramos, F. C., Hart, G. L., Patterson, J. D., & Brandon, A. D. (2008). Columbia River flood basalts from a centralized crustal magmatic system. *Nature Geoscience*, *1*(3), 177–180. https://doi.org/10.1038/ngeo124

Yale, L. B., & Carpenter, S. J. (1998). Large igneous provinces and giant dike swarms: Proxies for supercontinent cyclicity and mantle convection. *Earth and Planetary Science Letters*, *163*(1–4), 109–122. https://doi.org/10.1016/S0012-821X(98)00179-4

Ziou, D., & Tabbone, S. (1998). *Edge detection techniques—an overview* (pp. 1–41). Pria. Retrieved from http://nyx-www.informatik.uni-bremen.de/1044/1/ziou_pria_98.pdf

References From the Supporting Information

McKinney, W. (2011). pandas: A foundational python library for data analysis and statistics. *Python for High Performance and Scientific Computing*, *14*(9), 1–9.

pandas development team, T. (2020). *pandas-dev/pandas: Pandas* (Vol. 2). Zenodo. https://doi.org/10.5281/zenodo.3509134